Cell Reports

Article

Homeostatic PD-1 signaling restrains EOMES-dependent oligoclonal expansion of liver-resident CD8 T cells

Graphical abstract

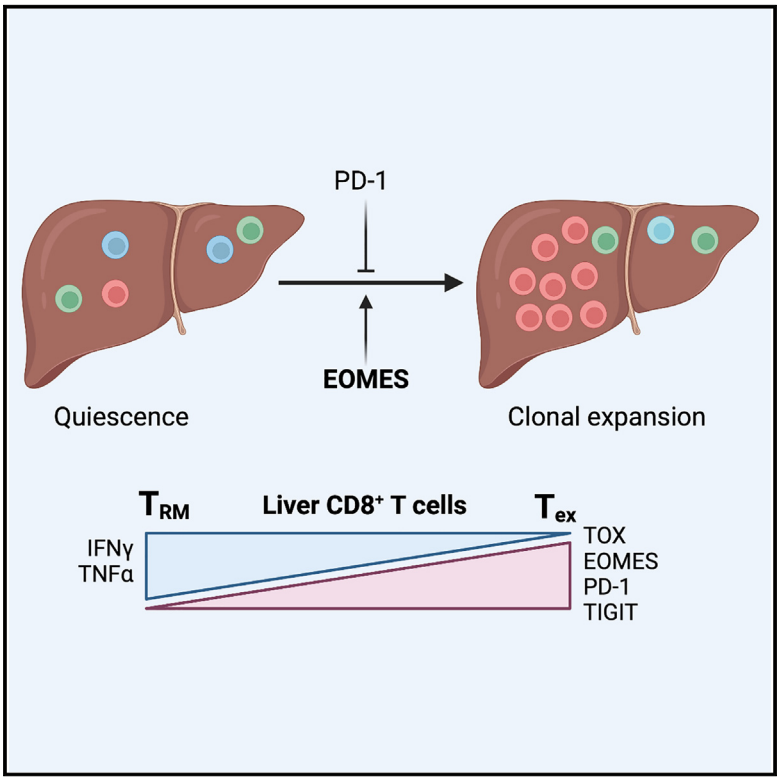

Authors

Marie Le Moine, Abdulkader Azouz, Guillem Sanchez Sanchez, ..., David Vermijlen, Fabienne Andris, Stanislas Goriely

Correspondence

stanislas.goriely@ulb.be

In brief

The physiological role of the PD-1 axis remains unclear. Le Moine et al. show that interfering with this pathway leads to a preferential clonal expansion of liver-resident CD8$^+$ T cells. These results could help to understand the mechanisms involved in immune-related adverse events in patients under checkpoint inhibitors.

Highlights

- PD-1 controls the homeostasis of hepatic memory CD8 T cells
- PD-1 blockade leads to an expansion of liver-resident CD8 T cells
- These cells are oligoclonal and display an exhaustion profile
- The transcription factor EOMES plays a central role in this process

Le Moine et al., 2023, Cell Reports *42*, 112876
August 29, 2023
https://doi.org/10.1016/j.celrep.2023.112876

CellPress

Cell Reports

CellPress
OPEN ACCESS

Article

Homeostatic PD-1 signaling restrains EOMES-dependent oligoclonal expansion of liver-resident CD8 T cells

Marie Le Moine,[1,2] Abdulkader Azouz,[1,2] Guillem Sanchez Sanchez,[1,2,4] Solange Dejolier,[2,3] Muriel Nguyen,[1,2] Séverine Thomas,[1,2] Valdrin Shala,[1,2] Hacene Dreidi,[2,3] Sébastien Denanglaire,[2,3] Frédérick Libert,[5] David Vermijlen,[1,2,4,6] Fabienne Andris,[2,3,7,8] and Stanislas Goriely[1,2,3,7,8,9,*]

[1]Institute for Medical Immunology (IMI), Université Libre de Bruxelles (ULB), Gosselies, Belgium
[2]ULB Center for Research in Immunology (U-CRI), ULB, Brussels, Belgium
[3]Immunobiology Lab, ULB, Gosselies, Belgium
[4]Department of Pharmacotherapy and Pharmaceutics, ULB, Brussels, Belgium
[5]Institute of Interdisciplinary Research (IRIBHM) and Brightcore, ULB, Brussels, Belgium
[6]WELBIO Department, WEL Research Institute, Avenue Pasteur, 6, 1300 Wavre, Belgium
[7]These authors contributed equally
[8]Senior author
[9]Lead contact
*Correspondence: stanislas.goriely@ulb.be
https://doi.org/10.1016/j.celrep.2023.112876

SUMMARY

The co-inhibitory programmed death (PD)-1 signaling pathway plays a major role in the context of tumor-specific T cell responses. Conversely, it also contributes to the maintenance of peripheral tolerance, as patients receiving anti-PD-1 treatment are prone to developing immune-related adverse events. Yet, the physiological role of the PD-1/PDL-1 axis in T cell homeostasis is still poorly understood. Herein, we show that under steady-state conditions, the absence of PD-1 signaling led to a preferential expansion of $CD8^+$ T cells in the liver. These cells exhibit an oligoclonal T cell receptor (TCR) repertoire and a terminally differentiated exhaustion profile. The transcription factor EOMES is required for the clonal expansion and acquisition of this differentiation program. Finally, single-cell transcriptomics coupled with TCR repertoire analysis support the notion that these cells arise locally from liver-resident memory $CD8^+$ T cells. Overall, we show a role for PD-1 signaling in liver memory T cell homeostasis.

INTRODUCTION

Immune-checkpoint blockade (ICB) represents a breakthrough in the treatment of cancer. In particular, interference with programmed death (PD)-1 signaling may restore CD8 T cell function in the tumor microenvironment, thereby allowing effective immune response and tumor control.[1,2] In the last decades, considerable efforts have allowed the identification of specific CD8 T cell subsets that are responsive to these treatments.[3]

In the context of acute infection, PD-1 expression increases rapidly and transiently upon T cell receptor (TCR) activation of CD8 T cells and acts as a rheostat during naive-to-effector transition.[4,5] In the context of chronic infection or cancer, sustained antigenic stimulation[6] and continuous TCR-mediated nuclear factor of activated T cell (NF-AT) signaling[7,8] favor the acquisition of an "exhausted" (exhausted T cell [Tex]) phenotype, characterized by progressive functional hyporesponsiveness and expression of inhibitory co-receptors, including PD-1, LAG3, TIGIT, and TIM-3 and the ectoenzymes CD38 and CD39.[9] Key transcription factors downstream of the TCR, such as the high-mobility group box DNA-binding protein TOX[10–13] and nuclear receptor subfamily 4A (NR4A) family members drive this program.[14] Furthermore, multiple studies identified a key role for the memory-related transcription factor T-cell factor (TCF)1 in maintaining the capacity to self-renew and to sustain the exhausted populations.[15–18] Expression of T-BET and EOMES, two related T-box transcription factors, is also highly regulated during this differentiation process, but their exact contribution remains poorly defined.[19–21] Altogether, two main states of CD8 T cell exhaustion have been observed: a precursor subset ($TOX^+PD\text{-}1^{int}TCF1^+TIM3^-T\text{-}bet^{hi}EOMES^{int}$) most abundantly found in secondary lymphoid tissues and able to differentiate in response to anti-PD-1 treatment and a terminally differentiated subset ($TOX^+PD\text{-}1^{hi}TCF1^-TIM3^+T\text{-}bet^{lo}EOMES^{hi}$) predominantly found in peripheral tissues or the tumor microenvironment that displays potential cytotoxic functions.[18] Expansion of T cell clones in response to ICB has been correlated with favorable outcome in patients with cancer.[22–27]

While the role of PD-1 signaling has been extensively studied in the context of cancer or chronic infection, the physiological role of this pathway during homeostasis remains unclear. Several lines of evidence indicate that PD-1 blockade interferes

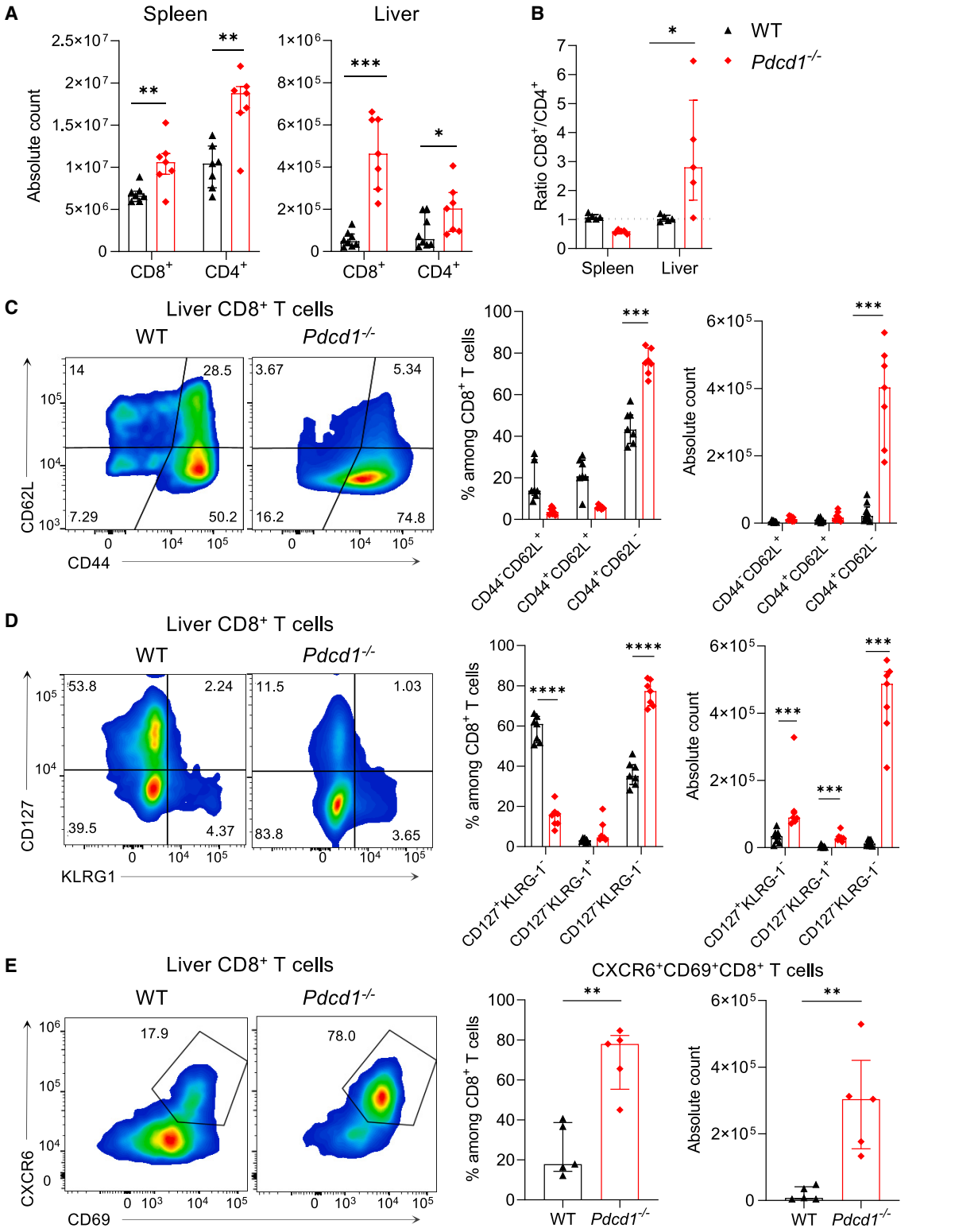

(legend on next page)

with T cell homeostasis. Indeed, patients with cancer under ICB can develop potentially life-threatening immune-related adverse events.[28,29] The phenotype of *Pdcd1*$^{-/-}$ mice includes moderate splenomegaly, increased B cell responses and late onset of lupus-like autoimmune disease or autoantibody-mediated cardiomyopathy, depending on the genetic background.[30,31] PD-1 signaling also contributes to CD8$^+$ T cell homeostasis, as mice with a non-functional PD-1/PDL1 axis display increased frequency of CD8$^+$ T cells in the liver under steady-state conditions and upon immunization.[32,33] Furthermore, Charlton et al. observed an accumulation of CD8$^+$ T cells with an effector memory (TEM) phenotype in lymphoid organs and tissues of *Pdcd1*$^{-/-}$ mice.[34]

Herein, we show that under steady-state conditions, the absence of PD-1 signaling leads to a highly preferential expansion of CD8$^+$ T cells within the liver. Strikingly, these expanded cells exhibited a pronounced oligoclonal TCR repertoire, which was associated with an exhausted profile. Using loss- or gain-of-function strategies, we could demonstrate that these clonal expansions were dependent on the transcription factor EOMES. Finally, we performed transcriptomic and epigenomic analysis to define their molecular features and to gain insight into their developmental trajectories. With these results, we uncovered an unexpected role for EOMES and PD-1 signaling in liver memory T cell homeostasis.

RESULTS

Expansion of activated CD69$^+$CD8$^+$ T cells in the spleen and liver of *Pdcd1*$^{-/-}$ mice

To understand the physiological role of the PD-1 signaling pathway, we evaluated the T cell compartment of 6- to 12-week-old *Pdcd1*$^{-/-}$ mice under steady-state conditions. Earlier works reported an accumulation of CD8$^+$ T cells in the spleen and liver in the absence of PD-1 or PD-L1, and we therefore initially focused our attention on these organs.[32–34] Consistent with previous reports, we observed moderate hepatosplenomegaly in *Pdcd1*$^{-/-}$ mice compared with their wild-type (WT) counterparts (Figure S1A).[30] Both CD8 and CD4 T cell counts were increased in the spleen and liver of *Pdcd1*$^{-/-}$ mice compared with WT mice (Figure 1A). However, by comparing the CD8-to-CD4 ratios in both strains and organs, we observed a preferential expansion of CD8$^+$ T cells in the liver of *Pdcd1*$^{-/-}$ mice (Figure 1B). To further define the phenotype of these cells, we examined the expression of different classical CD8$^+$ T cell markers. In both organs, we observed higher proportions and total counts of activated/effector memory CD62L$^-$CD44$^+$ T cells in *Pdcd1*$^{-/-}$ mice compared with WT mice (Figures 1C and S1B). In the liver of *Pdcd1*$^{-/-}$ mice, this subset represented more than 70% of all CD8$^+$ T cells. This massive expansion of hepatic CD62L$^-$CD44$^+$ T cells was compensated by a relative decrease in the proportion of CD62L$^+$CD44$^+$, which comprises both conventional central memory and CD49d^{lo} "virtual memory" cells (Figure S1E). Although we observed a relative decrease in the proportion of CD62L$^+$CD44$^+$ T cells, the absolute number of this subset was not decreased, suggesting that the expansion of CD8$^+$ T cells in *Pdcd1*$^{-/-}$ mice is not due to a global conversion of central to effector memory cells (Figure 1C).

Consistent with previous reports,[35] we observed the appearance of effector (CD127^{lo}KLRG1$^+$) cells in the spleen of *Pdcd1*$^{-/-}$ mice (Figure S1C). However, in the liver of these mice, the accumulation of CD8 T cells was mostly due to an expansion of CD127^{lo}KLRG1^{lo} cells, suggesting that they are not classical effector nor effector memory cells (Figure 1D).[36,37]

Besides effector and central memory T cells in the liver, the conventional memory CD8$^+$ T cell population consists of tissue-resident memory T cells (Trms).[38] Liver Trms are characterized by high expression of retention markers such as CXCR6, CD69, and CD49a.[39,40] We could observe an expansion of CXCR6$^+$CD69$^+$ T cells in the livers of *Pdcd1*$^{-/-}$ mice compared with WT mice (Figure 1E). This population was barely present in spleen of both strains, consistent with their tissue-resident profile (Figure S1D). However, the proportion of CD49a$^+$ T cells in *Pdcd1*$^{-/-}$ mice was decreased compared with WT mice, suggesting that the expanded T cell population expressed some retention markers but did not fit with a classical Trm phenotype (Figure S1F).[41]

In summary, we observed the preferential expansion of CD44$^+$CD62L$^-$CD127$^-$KLRG1$^-$CD49d$^+$ CD49a$^-$CD69$^+$CXCR6$^+$ CD8$^+$ T cells in the liver of *Pdcd1*$^{-/-}$ mice. As these cells did not express classical markers of memory nor effector T cells, we further evaluated their phenotypic and transcriptomic features.

Liver CD8$^+$ T cells that expand in *Pdcd1*$^{-/-}$ mice display features of exhaustion

We performed single-cell RNA sequencing on CD8 T cells from the spleens and livers of individual WT and *Pdcd1*$^{-/-}$ mice (3 mice/group). Of a total of 20,517 CD8 T cells, 12 clusters were identified in an unsupervised manner. Based on their transcriptional profiles, we annotated and grouped these clusters into 8 distinct subpopulations (Figure 2A; see also Figure S2A for expression of selected genes in uniform manifold approximation and projection [UMAP] plots). As expected, spleen CD8$^+$ T cells from WT mice were mainly enriched for naive (expressing *Sell*, *Lef1*, and *Tcf7*) and central memory cells (expressing *Id3*, *Sell*, and *Tcf7*). We also identified less abundant subsets that display activation features (*Nfkbia*, *Myc*, *Tnfrsf9*, *Nr4a1*) and express cell-cycle-related genes, a type I interferon (IFN) signature (IFN signaling-associated genes [ISAG]^{hi} subset expressing *Isg15*, *Ifit3*, and *Ifit1*), or a Tem subset (expressing *Klrg1*,

Figure 1. Expansion of activated CD69$^+$CD8$^+$ T cells in the spleen and liver of *Pdcd1*$^{-/-}$ mice

(A and B) Absolute counts (A) and relative ratio (B) of CD8$^+$ or CD4$^+$ T cells in spleens and livers of WT or *Pdcd1*$^{-/-}$ mice.

(C–E) Representative FACS plots, relative proportion of each subpopulation among CD8$^+$ T cells, and absolute counts in the livers of WT or *Pdcd1*$^{-/-}$ mice.

Results are given as median ± interquartile range and are representative of 2–3 independent experiments (n = 3–5 mice per group). Each dot represents an individual mouse. Statistical significance was assessed by the Mann-Whitney test (*p < 0.05, **p < 0.01, ***p < 0.001, ****p < 0.0001).

See also Figure S1.

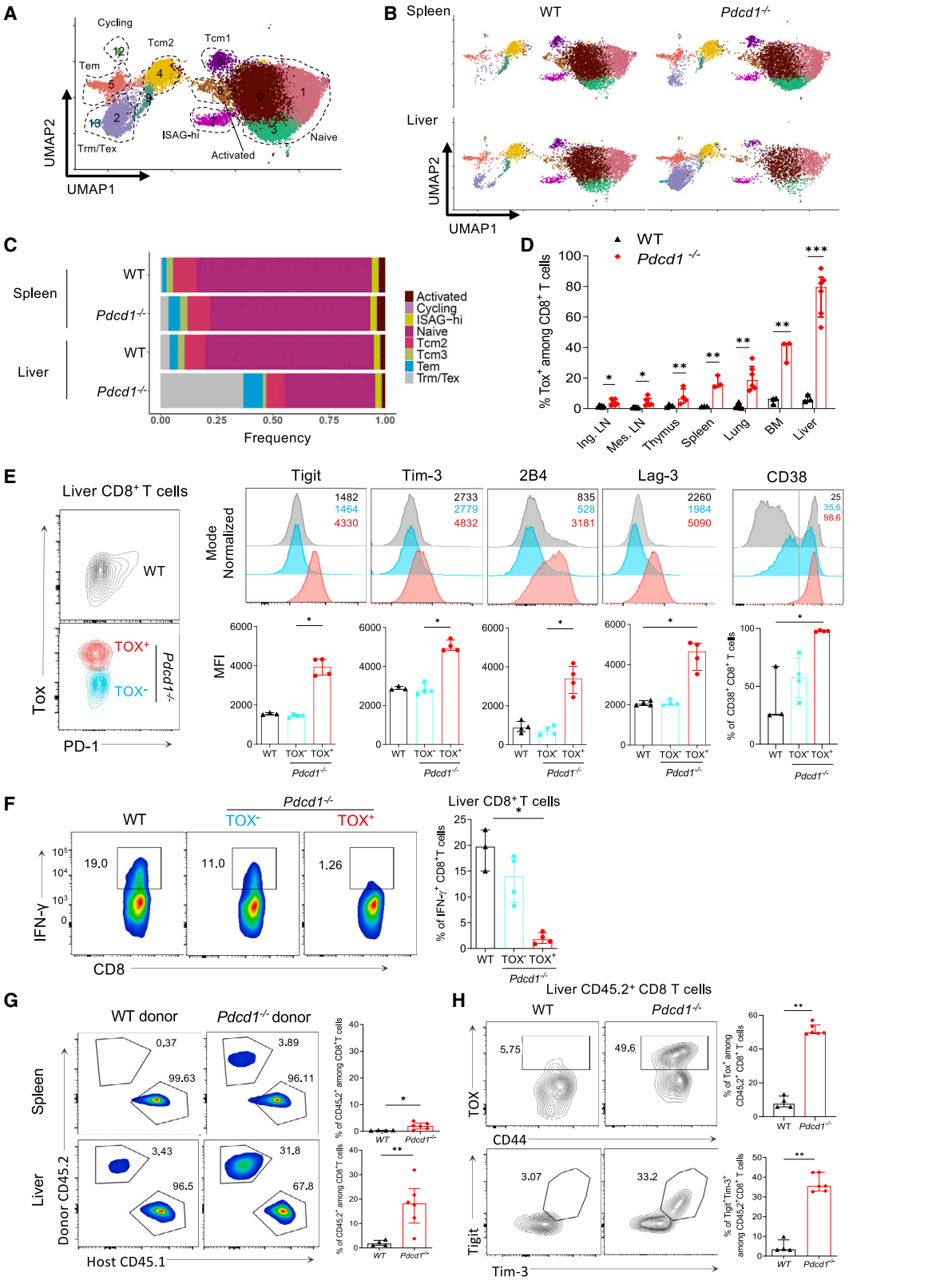

(legend on next page)

Cxcr3, *Tbx21*, and *Top2a*). In WT livers, we observed an increased proportion of the Tem cluster and also identified a subset that expressed both tissue-resident memory (*Itga1*, *Cxcr6*) and exhaustion-related features (*Tox*, *Tigit*, *Nr4a2*, *Ctla4*) that accounted for 4% of CD8$^+$ T cells. In both spleen and liver of *Pdcd1*$^{-/-}$ mice, we observed a modest increase in the frequency of Tems in comparison to their WT counterparts (Figure 2B). The most striking feature, however, was a major expansion of the liver Trm/Tex cluster (Figures 2B and 2C). Pairwise comparison of WT versus *Pdcd1*$^{-/-}$ cells from this subset revealed higher expression of genes related to effector functions (such as *Gzma*, *Gzmk*, and *Ccl5*). We also noticed upregulation of *Tox*, a transcription factor involved in the acquisition of exhaustion features,[10–12,14] and a reduced expression of residency-associated genes (such as *Zfp683* [encoding Hobit], *P2rx7*, or *Itga1*) (Figure S2B). A similar comparison of the Tem CD8 subset revealed few differentially expressed genes, indicating that in the absence of PD-1 signaling, their increased frequency was not accompanied by strong reprograming. We nevertheless also identified higher expression of *Tox* and effector genes in *Pdcd1*$^{-/-}$ cells (Figure S2B).

Fluorescence-activated cell sorting (FACS) analysis confirmed the appearance of an abundant TOX$^+$CD8$^+$ T cell population in *Pdcd1*$^{-/-}$ mice that was virtually absent in the WT strain (Figure S3A). TOX$^+$CD8$^+$ T cells were also detected in lymphoid and other non-lymphoid organs from *Pdcd1*$^{-/-}$ mice but accounted for the majority of CD8$^+$ T cells in the liver of these mice (Figure 2D). Next, we evaluated the surface expression of co-inhibitory receptors and ectoenzymes. We systematically observed higher expression of TIGIT, Tim-3, 2B4, Lag-3, CD38, and CD39 along with lower expression of CD127, KLRG1, or CD49a in TOX$^+$ CD8 T cells from the livers of *Pdcd1*$^{-/-}$ mice compared with their TOX$^-$ counterparts or with total CD8$^+$ T cells from the livers of WT mice (Figures 2E, S3B, and S3C). Moreover, TOX$^+$ CD8 T cells expressed high levels of the retention markers CD69 and CXCR6 (Figure S3D). To evaluate their functionality, we performed *ex vivo* stimulation with PMA and ionomycin. We observed that TOX$^+$ CD8$^+$ T cells from the livers of *Pdcd1*$^{-/-}$ mice produced reduced levels of IFN-γ compared with their TOX$^-$ counterparts or with CD8$^+$ T cells from the liver of WT mice, consistent with their "exhausted" phenotype (Figure 2F). In contrast, the CD8$^+$ T cells from the spleen of *Pdcd1*$^{-/-}$ mice did not display differences in functionality in comparison to their WT counterparts (Figure S3E).

To evaluate the cell-intrinsic role of PD-1 signaling, we adoptively transferred polyclonally activated CD8$^+$ splenocytes from WT and *Pdcd1*$^{-/-}$ mice into congenic WT hosts. Two weeks post-transfer, we observed a clear expansion of liver TOX$^+$ Tigit$^+$Tim-3$^+$CD8$^+$ T cells from *Pdcd1*$^{-/-}$ donors but not from WT donors (Figures 2G, 2H, and S4). Finally, we also performed experiments in WT mice using blocking PD-1 antibodies. After repeated injections over 2 weeks, we observed the expansion of TOX$^+$ CD8$^+$ T cells in the liver and, to a lesser extent, in the spleen (Figure S5A). These cells expressed high levels of PD-1 along with other co-inhibitory receptors, and developed less multi-cytokine secretion, compared with their TOX$^-$ counterparts or with CD8$^+$ T cells from untreated mice. They also expressed high levels of Ki67, which indicates strong local proliferation (Figures S5B–S5D). Taken together, these results indicate that continuous CD8 T cell-intrinsic PD-1 signaling in the liver is required to restrain their proliferation and acquisition of exhaustion features.

The expansion of liver CD8$^+$ T cells in the absence of PD-1 signaling is highly oligoclonal and private

Under steady-state conditions, we hypothesized that PD-1 signaling could preferentially restrain the expansion of CD8 T cells expressing specific TCR rather than having a global impact on T cell homeostasis. To evaluate the clonality of the CD8$^+$ T cells that expand in the absence of PD-1 signaling, we first stained CD8$^+$ T cells with commercially available Vβ antibodies (identifying a part of the Vβ repertoire) and calculated a Gini TCR skewing index[42] in WT and *Pdcd1*$^{-/-}$ mice. There was a clear skewing of the Vβ usage in liver CD8$^+$ T cells from *Pdcd1*$^{-/-}$ mice, while there was no such effect in the spleen compartment (Figure 3A). This skewing in the *Pdcd1*$^{-/-}$ mice was restricted to the TOX$^+$ subset (Figure 3B). In line with this observation, there was no skewing difference between activated CD44^{hi} in TOX$^-$ subsets from WT and *Pdcd1*$^{-/-}$ strains (Figure S6A). To have a more global and unbiased view on the TCR repertoire, we coupled single-cell TCR sequencing (scTCR-seq) to scRNA-seq analysis of CD8 T cells from WT and *Pdcd1*$^{-/-}$ strains described in Figure 2. We observed that the Trm/Tex cluster that arises in the liver of *Pdcd1*$^{-/-}$ mice was highly enriched for hyperexpanded clones (Figures 4C and

Figure 2. Liver CD8$^+$ T cells that expand in *Pdcd1*$^{-/-}$ mice display features of exhaustion

(A) Uniform manifold approximation and projection (UMAP) plots of CD8$^+$ T cells from the spleens and livers of WT and *Pdcd1*$^{-/-}$ mice segregated into 12 transcriptional clusters and 8 annotated populations according to their patterns of gene expression.

(B and C) UMAP plots split by sample (B) and proportions of cells in each annotated population (C).

(D) Proportion of TOX$^+$ T cells among CD8$^+$ T cells in lymphoid and non-lymphoid organs from WT and *Pdcd1*$^{-/-}$ mice. LN, lymph node.

(E) Representative FACS plots of TOX and PD-1 in CD8$^+$ liver T cells from WT and *Pdcd1*$^{-/-}$ mice with color codes. Expression of co-inhibitory receptors in WT CD8$^+$ T cells and in TOX$^-$ and TOX$^+$ *Pdcd1*$^{-/-}$ CD8$^+$ T cells. Histograms represent median fluorescence intensity (MFI) or the proportion of positive cells among the aforementioned subpopulations.

(F) Representative FACS plots and proportion of IFN-γ after PMA/ionomycin stimulation of WT liver CD8$^+$ T cells and of TOX$^-$ and TOX$^+$ CD8$^+$ T cells from the livers of *Pdcd1*$^{-/-}$ mice.

(G) Frequency of adoptively transferred WT or *Pdcd1*$^{-/-}$ CD45.2 CD8$^+$ T cells in the spleen and liver of CD45.1 WT mice.

(H) Expression of the indicated marker in WT or *Pdcd1*$^{-/-}$ adoptively transferred (CD45.2$^+$) CD8$^+$ T cells harvested from the liver.

Results are representative of 2–3 independent experiments (n = 3–6 mice per group) and are given as median ± interquartile range. Each dot represents an individual mouse. Statistical significance (*p < 0.05, **p < 0.01, ***p < 0.001) was assessed by the Mann-Whitney (D, G, and H) or the Kruskal-Wallis test (E and F). See also Figures S2–S5.

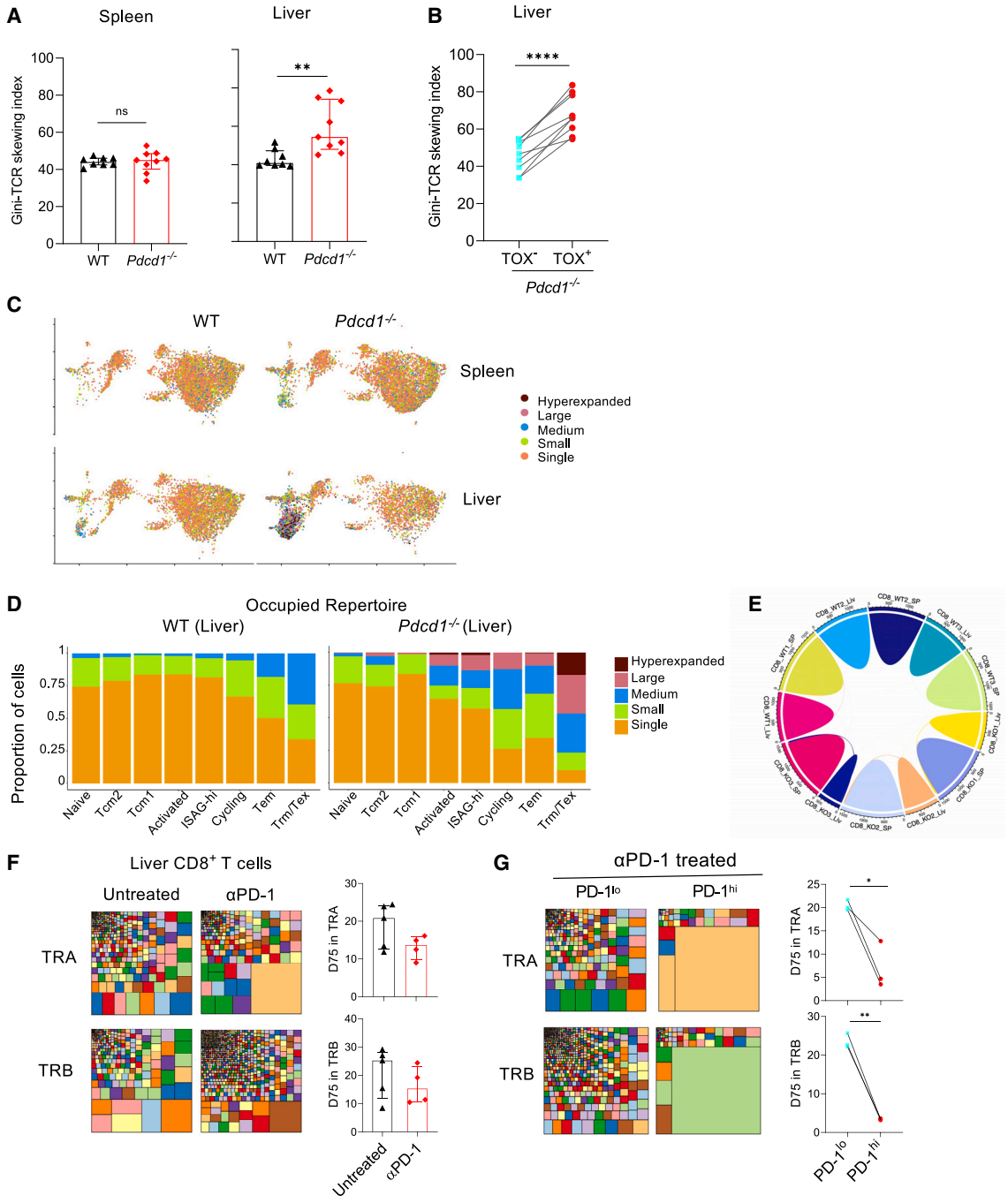

Figure 3. The expansion of liver CD8$^+$ T cells in the absence of PD-1 signaling is highly oligoclonal and private

(A) Gini TCR skewing index of splenic (right) or hepatic (left) CD8$^+$ T cells from WT and *Pdcd1*$^{-/-}$ mice.

(B) Gini TCR skewing index of hepatic TOX$^+$ and TOX$^-$ CD8$^+$ T cells from *Pdcd1*$^{-/-}$ mice.

(C) UMAP visualization of the clonal size assessed by scTCR-seq of the α and β chains.

(D) Fraction of the repertoire occupied by clonotypes according to their size in each annotated population in WT and *Pdcd1*$^{-/-}$ livers.

(E) Circos plots representing the degree of clonal sharing between organs and mice. Each line represents one shared clone.

(F) (Left) Tree map representations of the TRA and TRB repertoires of bulk CD8$^+$ liver T cells from untreated and treated mice with anti-PD-1 (colors used are random; no correspondence between graphs) and (right) D75 (percentage of clonotypes required to occupy 75% of the total TCR repertoire) analysis comparing the hepatic CD8$^+$ cells from WT and anti-PD-1-treated mice.

(legend continued on next page)

4D). We also noted some degree of clonal expansion among the cycling and Tem clusters from *Pdcd1*$^{-/-}$ mice. Importantly, hyperexpanded clonotypes differed among *Pdcd1*$^{-/-}$ mice, which indicates private expansions (Figure 3E).

To confirm these observations, we performed TCR repertoire analysis on bulk liver PD-1^{hi} (TOX^{+}) versus PD-1^{lo} (TOX^{-}) CD8^{+} T cells from anti-PD-1-treated mice (5 mice/group). A trend for increased clonality could be observed when total liver CD8^{+} T cells of anti-PD-1-treated mice were compared with untreated controls but not in the thymus spleen or blood (Figures 3F, S6B, and S6C). Liver PD-1^{hi} CD8^{+} T cells of anti-PD-1-treated mice showed a striking contraction of the breath of TRA and TRB repertoires, resulting in the presence of hyperexpanded clonotypes (Figures 3G, S5D, and S5E). The hyperexpanded clonotypes could only be occasionally traced back at very low frequencies in PD-1^{lo} cells and other tissues from the same mice (Figure S5F). Again, hyperexpanded clonotypes differed among anti-PD-1-treated mice (Figure S5G). In summary, interference with PD-1 signaling results in a highly oligoclonal and private expansion of liver-resident CD8^{+} T cells.

The expansion of Tex CD8^{+} T cells upon anti-PD-1 treatment is EOMES dependent

To gain further insight into the molecular mechanisms that drive this clonal expansion, we evaluated the expression of different transcription factors associated with the exhaustion differentiation pathway. We noticed that the expanded Trm/Tex cluster that arised in *Pdcd1*$^{-/-}$ mice largely expressed *Eomes* (Figure 4A). We next confirmed that TOX^{+} CD8 T cells from the liver of *Pdcd1*$^{-/-}$ mice homogeneously expressed high levels of EOMES, while its expression in TOX^{-} counterparts or WT CD8^{+} T cells was bimodal (Figures 4B and S7A). In contrast, expression of T-bet was comparable among these 3 groups (Figure 4B). These TOX^{+} T cells were also found to be negative for TCF1. Together with their high expression of Tim-3 and low production of IFN-γ, this is strongly suggestive that these cells have reached terminally Tex differentiation (Figure S7B).[16–18] As liver TOX^{+} CD8^{+} T cells also expressed high levels of EOMES upon PD-1 blockade (Figure 4C), we evaluated the role of this transcription factor in this experimental setting. We treated CD4Cre^{+}*Eomes*$^{fl/fl}$ mice (*Eomes*$^{\Delta/\Delta}$) and their control littermates (CD4Cre^{-}*Eomes*$^{fl/fl}$ mice [*Eomes*$^{fl/fl}$]) with anti-PD-1 monoclonal antibodies (mAbs). Strikingly, we observed that the expansion of hepatic TOX^{+}PD-1^{+} CD8 T cells that is triggered by PD-1 blockade was abrogated in *Eomes*$^{\Delta/\Delta}$ mice (Figure 4D). While differences between splenic CD8^{+} T cells from *Eomes*$^{fl/fl}$ and *Eomes*$^{\Delta/\Delta}$ upon PD-1 blockade were much less pronounced than their counterparts in the liver, they followed a similar trend (Figure S7C). To evaluate whether the role of EOMES is CD8 T cell autonomous, we generated chimeras by reconstituting irradiated *Rag2*$^{-/-}$ recipient mice with a 1:1 mixture of congenitally marked bone marrow cells from WT and *Eomes*$^{\Delta/\Delta}$ donor mice. *Eomes*-deficient CD8^{+} T cells displayed a reduced potential to develop into liver PD-1^{+}TOX^{+} T cells following anti-PD-1 treatment compared with their WT counterparts (Figure S8). Collectively, these results demonstrate that the expansion and acquisition of exhaustion features by liver CD8^{+} T clones upon PD-1 blockade are dependent on cell-autonomous EOMES expression.

Transgenic expression of EOMES leads to the expansion of liver Tex CD8^{+} T cells under steady-state conditions

To further define the role of EOMES in this process, we took advantage of a transgenic mouse strain that expresses *Eomes* under the control of hCD2 regulatory elements (named *Eomes*$^{Tg/Tg}$). In these mice, T cells express EOMES under steady-state conditions but at levels that remain in a physiological range (Figure 5A). We observed the spontaneous development of a TOX^{+}PD-1^{+} CD8 T cell population in the liver and, to a much lesser extent, in the spleen of *Eomes*$^{Tg/Tg}$ mice (Figures 5B and S9A). Also, EOMES levels of TOX^{+} T cells in *Eomes*$^{Tg/Tg}$ and in *Pdcd1*$^{-/-}$ mice were higher than in *Eomes*$^{Tg/Tg}$ TOX^{-} cells (Figure 5C), indicating that expression of the endogenous gene in TOX^{+} cells from *Pdcd1*$^{-/-}$ mice exceeds the levels reached by the transgene.

Phenotypic and functional features of TOX^{+} CD8^{+} T cells from *Eomes*$^{Tg/Tg}$ mice were very similar to the characteristics of these cells in *Pdcd1*$^{-/-}$ mice or upon anti-PD-1 treatment of WT mice: they expressed the retention markers CD69 and CXCR6, along with high levels of co-inhibitory receptors, were Tbet^{+} and TCF1^{lo}, and displayed reduced capacity to produce IFN-γ compared with their TOX^{-} counterparts or with WT CD8^{+} liver T cells (Figures S9B–S9H). While we did not detect a significant difference in Vβ usage in splenic and hepatic WT versus *Eomes*$^{Tg/Tg}$ in bulk CD8^{+} T cells (Figures 5D and S9I), we observed a higher TCR skewing in TOX^{+} CD8^{+} T cells compared with their TOX^{-} counterparts within *Eomes*$^{Tg/Tg}$ mice (Figure 5D, right panel). In sum, these results show that artificially maintaining EOMES expression in T lymphocytes is sufficient to lead to the expansion of CD8^{+} T cell clones even without subsequent PD-1 blockade.

To evaluate the role of TCR signaling in this context, we generated OT1 TCR transgenic mice on a *Rag1*$^{-/-}$ *Eomes*$^{Tg/Tg}$ background. These mice have a monoclonal T cell population that is specific for the SIINFEKL peptide of the OVA protein and constitutively expresses high levels of EOMES. In contrast to the *Eomes*$^{Tg/Tg}$ polyclonal T cell mice, *OT1*$^{+/+}$*Rag*$^{-/-}$*Eomes*$^{Tg/Tg}$ did not develop spontaneous TOX^{+}PD-1^{+} liver CD8^{+} T cells, suggesting the need for specific TCR signaling in combination with sustained EOMES expression for the development of hepatic TOX^{+} Texs (Figure 5E). Next, we infected WT and *Eomes*$^{Tg/Tg}$ mice with an attenuated Listeria strain expressing OVA (*Lm-OVA*$^{\Delta Acta}$). As this acute infection is self-limited, it allows us to study the impact of sustained EOMES expression in

(G) (Left) Tree map representations of the TRA and TRB repertoires of PD-1^{lo} and PD-1^{hi} CD8^{+} T cells from anti-PD-1-treated mice and (right) paired comparison of D75 values of PD-1^{lo} and PD-1^{hi} CD8^{+} T cells.

Statistical significance (*p ≤ 0.05, **p ≤ 0.01, ****p < 0.0001) was assessed by the Mann-Whitney test (A) or Wilcoxon matched-pair signed rank test (B and G). Results are given as median ± interquartile range, and each dot represents an individual mouse (A, B, and F).

See also Figure S6.

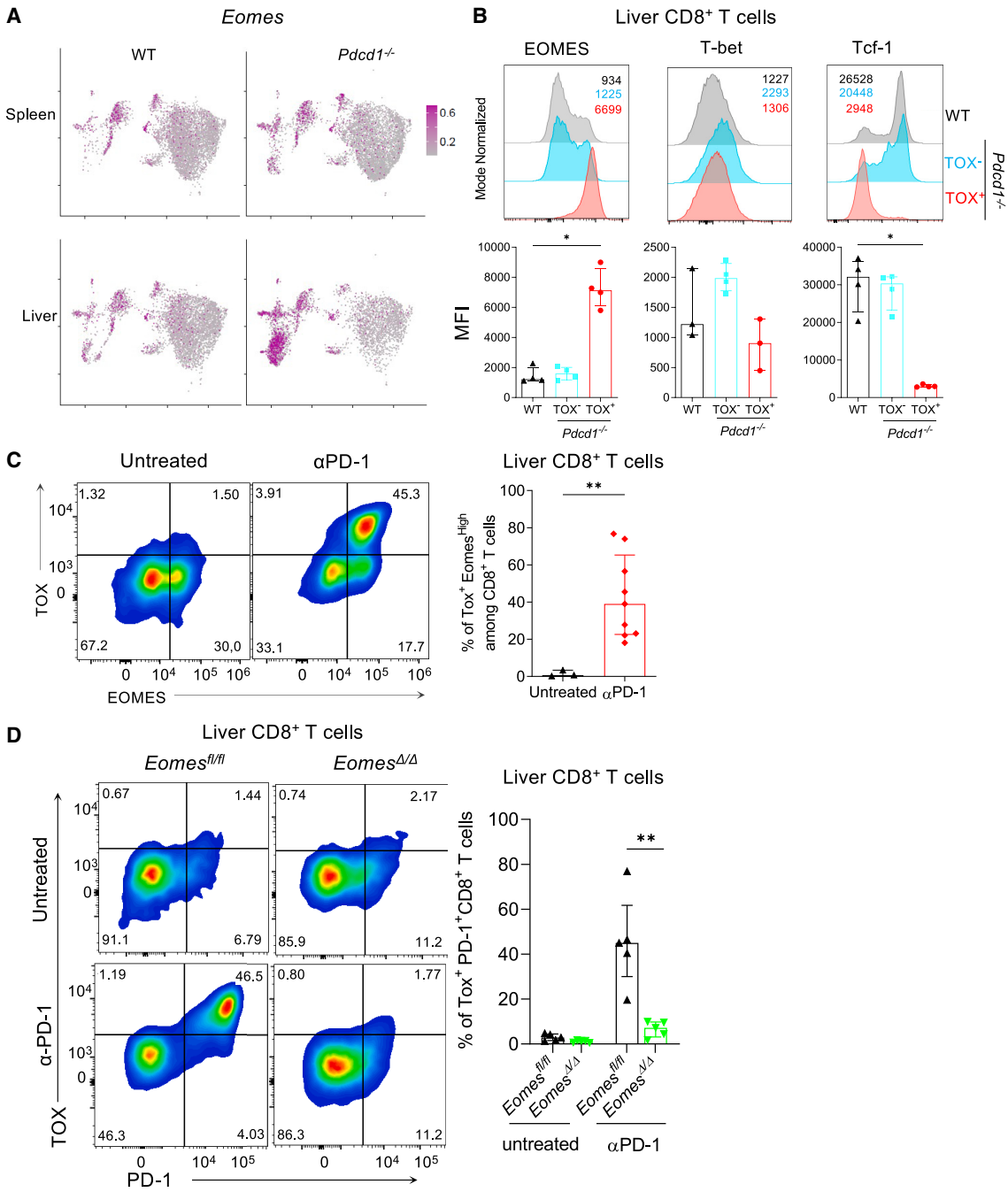

Figure 4. The expansion of Tex CD8$^+$ T cells in the absence of PD-1 signaling is Eomes dependent

(A) UMAP plots showing absolute expression (log-normalized count) of *Eomes* in cells from spleen and liver of WT and *Pdcd1*$^{-/-}$ mice.

(B) Representative FACS histograms and MFI of EOMES, T-bet, and TCF1 in hepatic WT CD8$^+$ T cells or in Tox$^-$ and Tox$^+$ CD8$^+$ T cells from the livers of *Pdcd1*$^{-/-}$ mice.

(C) Representative FACS plots and proportion of Tox$^+$Eomes^{hi} T cells among liver CD8$^+$ T cells in WT mice treated or not with αPD-1.

(D) *Eomes*$^{fl/fl}$ and *Eomes*$^{\Delta/\Delta}$ (*Eomes*$^{fl/fl}$ CD4-Cre) mice were treated or not with αPD-1 as in (C). Representative FACS plots and proportion of liver TOX$^+$ PD-1$^+$ T cells CD8$^+$ T cells in each group.

Representative of 2–3 independent experiments (n = 4–5 mice per group). Results are given as median ± interquartile range, and each dot represents an individual mouse. Statistical significance (*p < 0.05, **p < 0.01, ***p < 0.001) was assessed by the Mann-Whitney test (B and C) or the Kruskal Wallis test (A).

See also Figures S7 and S8.

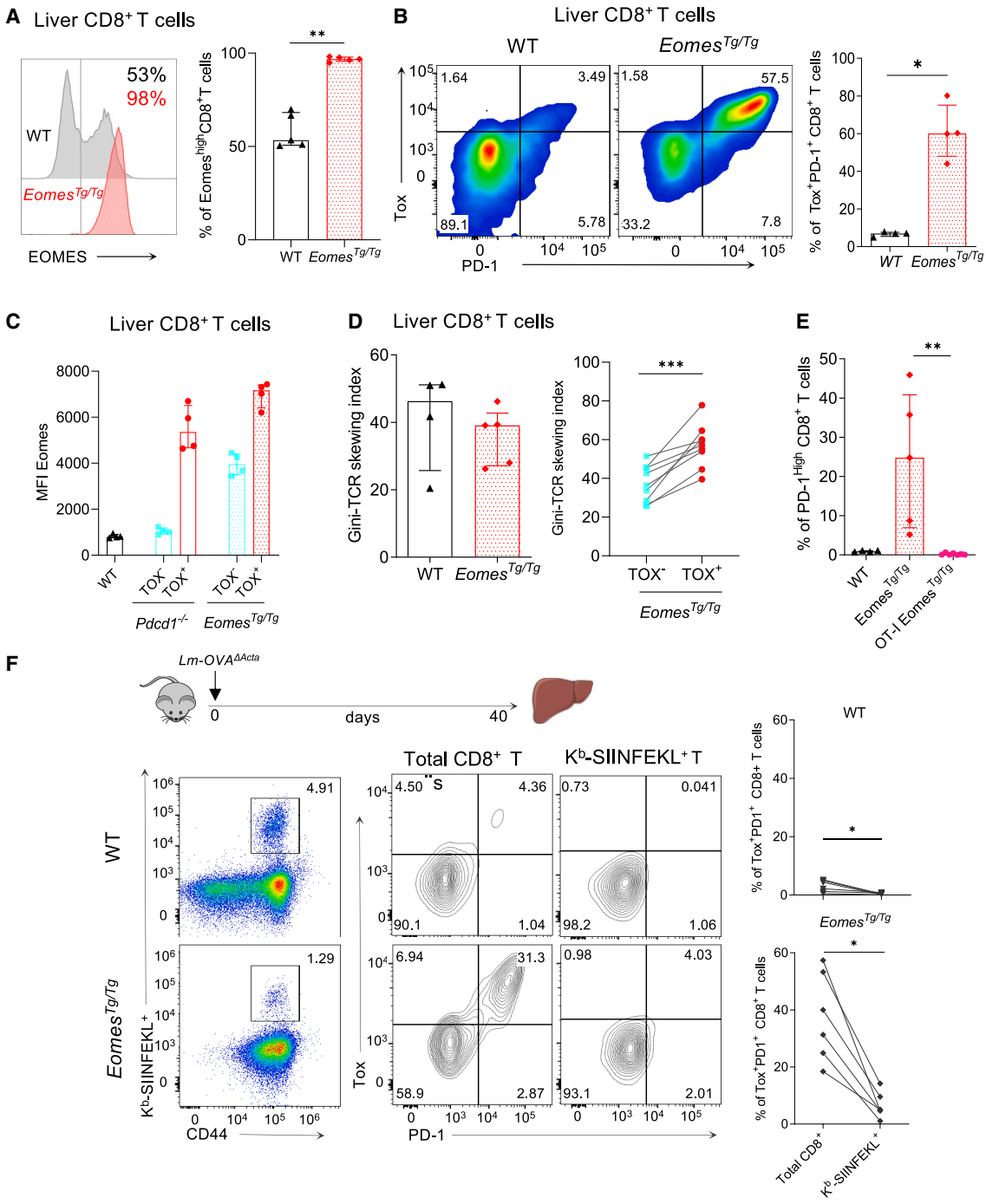

Figure 5. Transgenic expression of EOMES leads to the expansion of liver Tex CD8⁺ T cells under steady-state conditions

(A) Representative FACS histograms and proportion of EOMES^{hi}CD8$^+$ T cells in the livers of WT or *Eomes*$^{Tg/Tg}$ mice.

(B) Representative FACS plot and proportions of TOX$^+$PD-1$^+$ CD8$^+$ T cells in the livers of WT or *Eomes*$^{Tg/Tg}$ mice.

(C) MFI of EOMES in WT CD8$^+$ T cells or in TOX$^-$ and TOX$^+$ CD8 T cells from *Pdcd1*$^{-/-}$ or *Eomes*$^{Tg/Tg}$ mice.

(D) Gini TCR skewing index of bulk liver CD8$^+$ T cells from WT or *Eomes*$^{Tg/Tg}$ mice and from TOX$^-$ and TOX$^+$ CD8$^+$ T cells from *Eomes* $^{Tg/Tg}$ mice.

(E) Proportion of PD-1^{hi} cells among CD8$^+$ T cells from the livers of WT, *OT-1*$^{+/+}$*Rag*$^{-/-}$*Eomes*$^{Tg/Tg}$, and *Eomes*$^{Tg/Tg}$ mice.

(F) *Listeria monocytogenes* (Lm)$^{\Delta Acta\text{-}Ova}$ infection in WT and *Eomes*$^{Tg/Tg}$ mice. Livers were harvested and analyzed 40 days after infection. Representative FACS plot of K^b-SIINFEKL$^+$ T cells in each strain and expression of TOX and PD-1 gated on total or K^b-SIINFEKL$^+$ CD8$^+$ T cells.

(legend continued on next page)

bona fide OVA-specific memory CD8 T cells 40 days after the initial challenge (Figure S9J).[43,44] As expected, at this time point, K^b-SIINFEKL$^+$ CD8$^+$ T cells in the liver of WT mice did not express TOX nor PD-1, as this profile requires persistent antigenic stimulation (Figure 5F). Strikingly, K^b-SIINFEKL$^+$ CD8$^+$ T cells from *Eomes*$^{Tg/Tg}$ mice were also found exclusively among TOX$^-$PD-1$^-$. Taken together, these data strongly suggest that TOX$^+$ T cells that expand in an EOMES-dependent manner require persistent TCR signaling.

Epigenetic profile of EOMES-driven Tex CD8$^+$ T cells

To further decipher the mechanisms involved in EOMES-dependent acquisition of exhaustion features, we performed assay for transposase accessible chromatin (ATAC)-seq experiments on sorted PD-1^{hi} and PD-1^{lo} CD8$^+$ T cells from the liver of *Eomes*$^{Tg/Tg}$ mice along with their WT (PD-1^{lo}) counterparts. This allowed us to evaluate their epigenetic landscapes. We observed major differences in the accessibility of chromatin regions between *Eomes*$^{Tg/Tg}$ PD-1^{hi} cells and PD-1^{lo} cells (Figure S10A). In contrast, the impact of the EOMES transgene in PD-1^{lo} (*Eomes*$^{Tg/Tg}$ PD-1^{lo} versus WT) cells was more limited.

In order to position the epigenetic program of *Eomes*$^{Tg/Tg}$ PD-1^{hi} cells, we evaluated the overlap between these differentially accessible regions and well-defined epigenetic signatures that were defined based on a unified atlas of chromatin accessibility of CD8$^+$ T cells across multiple studies.[45,46] As expected, regulatory elements associated with a naive state were found among less accessible regions of *Eomes*$^{Tg/Tg}$ PD-1^{hi} cells (Figure S10B). This was also the case for regions associated with central memory, memory precursor, or TCF1$^+$ progenitor-like states. Signatures of effector or resident memory states were enriched in both conditions. In sharp contrast, regions specifically identified in terminally dysfunctional cells were exclusively found in more accessible regions. This analysis indicates that liver PD-1^{hi} cells that spontaneously arise under the influence of EOMES adopt a terminally dysfunctional/exhaustion differentiation program.

Regions that were less accessible in PD-1^{hi} cells were enriched for TCF, Krüppel-like factors (KLF), and ymphoid enhancer factor (LEF) binding motifs (Figure S10C). This is consistent with the notion that these transcription factors are more active in naive and central memory cells than in terminally differentiated cells. In agreement with their exhausted phenotype, regions that were more accessible in PD-1^{hi} cells were strongly enriched for NR4A-, NFAT-, and AP1-related motifs.[45] Importantly, we also identified T-box binding sites, suggesting that EOMES directly contributes to this differentiation program. Along this line, a substantial portion of chromatin immunoprecipitation (ChIP)-seq peaks identified for EOMES in the context of lymphocytic choriomeningitis virus (LCMV) infection[47] overlapped with the regions that are more or less accessible in PD-1^{hi} cells (52% and 25%, respectively) (Figure S10D). EOMES-bound regulatory regions that were more accessible in PD-1^{hi} cells were clearly associated with genes involved in lymphocyte differentiation and cell survival (Figure S10E). Indeed, we identified key genes that could represent direct targets of EOMES in this context, including *Pdcd1* itself, *Tox*, *Tox2*, *Nr4a2*, and the pro-survival gene *Bcl2* (Figure S10F). These data confirm the notion that EOMES participates in the core transcriptional network of Texs.

Transgenic expression of EOMES promotes the expansion of liver CD8$^+$ T clones with an exhaustion profile and resident memory features

To further decipher the developmental pathway leading to the acquisition of a Tex profile upon transgenic EOMES expression, we performed scRNA-seq coupled with TCR-seq on 18,675 CD8 T cells from the spleens and livers of WT and *Eomes*$^{Tg/Tg}$ mice. Based on their transcriptional profiles, we annotated and grouped the UMAP clusters into 11 distinct subpopulations (Figures 6A–6C), as defined in Figure 2. The Trm/Tex subset could be split into distinct clusters with dominant Trm or Tex profiles. In line with our previous experiments, we observed a major expansion of specific clusters that display Tex features in the liver of *Eomes*$^{Tg/Tg}$ mice (Figure 6B). As expected, CD8$^+$ T cells from *Eomes*$^{Tg/Tg}$ mice exhibited high expression of *Eomes*, with the highest levels in the Tex subsets (Figure 6C, top panels). In WT mice, we observed high expression of *Eomes* in the Tcm, Tem, activated, and ISAG^{hi} clusters, in accordance with the role of EOMES in effector and memory T cells.[48] Almost no expression was observed in Trm subsets from WT mice (Figure 6C). Tex clusters exhibited high expression of *Pdcd1*, *Tigit*, *Havcr2* (encoding TIM-3), and *Tox* and low expression of *Tcf7* or *S1pr1*. *Tbx21* expression was mainly enriched in Tems and a subset of Trms. Expression of *Zfp683* (encoding HOBIT) was enriched in Trm clusters and was absent in the other populations, in agreement with its role for the development of this subset (Figure 6C).[49,50] An effector memory gene signature[51] was specifically enriched in ISAG^{hi} and Tem subsets and was found to be low in Trm1s and Texs (Figure 6D, bottom panel). In agreement with data obtained in *Pdcd1*$^{-/-}$ mice, an exhaustion gene signature,[51] which was strongly enriched in the Tex subset, was also enriched in Trm1s and cycling cells. Conversely, a resident memory gene signature,[52] which was enriched in Trm clusters, was also present in Texs, in line with their retention profile. Moreover, the Trm/Tex signature identified in Figure 2 was strongly enriched in the Trm and Tex subsets defined in this setting (Figure 6D, top panel).

Finally, to gain more insight into the potential developmental pathways, we performed trajectory analysis using Slingshot.[53] By taking naive cells as a root, we identified four different trajectories, with two (lineages 2 and 4) of them ending in Tcm clusters. Lineage 3 ended in the cycling cluster. Importantly, in the lineage 1 differentiation trajectory, naive T cells first acquire activation (activated to ISAG^{hi} clusters), then memory (effector to resident memory clusters), and finally exhaustion features (Tex clusters)

Results are given as median ± interquartile range and are representative of at least two independent experiments (n = 4–5 mice per group) (excepting F, only performed once with 6 mice/group). Each dot represents an individual mouse; Statistical significance (*p < 0.05, **p < 0.01, ***p < 0.001) was assessed by the Mann-Whitney test (A, B, and E) or the Wilcoxon matched-pair signed rank test (D and F).
See also Figures S9 and S10.

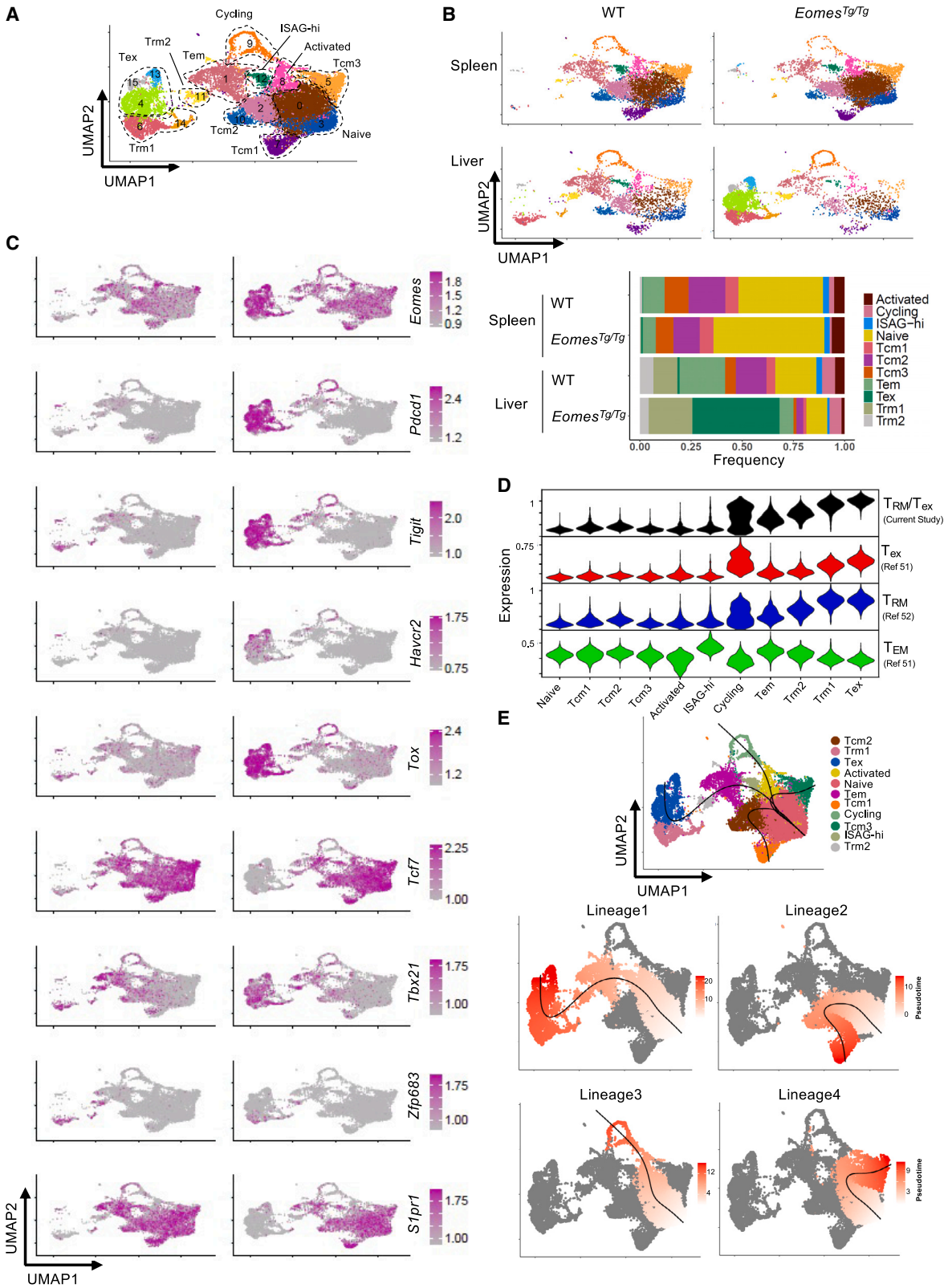

(legend on next page)

(Figures 6E and S11). These findings support a strong developmental link between Trms that physiologically arise in the liver under homeostatic conditions and Texs that accumulate under the influence of EOMES.

In the same single-cell experiment, we analyzed the TCR repertoire to evaluate the potential relationship between the subsets at the clonal level. In line with our bulk TCR-seq data on anti-PD-1-treated animals and scTCR-seq data on *Pdcd1*$^{-/-}$ mice, we observed that the Tex clusters that arise in the liver of *Eomes*$^{Tg/Tg}$ mice were highly enriched for hyperexpanded clones (Figures 7A and 7B). We also noted some degree of clonal expansion among the cycling, Tem, and the Trm1 clusters both in WT and *Eomes*$^{Tg/Tg}$ mice. By using different diversity scores, we observed that the *Eomes*$^{Tg/Tg}$ hepatic T cells accounted for the least diverse T cell population (Figure 7C). The 10 most abundant clonotypes of *Eomes*$^{Tg/Tg}$ liver T cells were not found among splenic cells from the same animals, supporting the notion that their expansion is a local process and that they do not recirculate (Figure 7D). We observed that in WT liver, clonotypes identified in a given subset were rarely shared with other subsets (except for cycling cells, which do not represent an independent functional program). In sharp contrast, we observed a very important promiscuity among subsets in the liver of *Eomes*$^{Tg/Tg}$ mice, as Tex hyperexpanded clones were also detected among Tem, cycling, and Trm subsets (Figure 7E). These experiments strongly support the notion that transgenic EOMES expression interfered with the PD-1-driven quiescent state of specific liver-resident memory T cell clones and promoted their expansion and exhaustion profile.

DISCUSSION

In the present study, we have identified a role for the PD-1 pathway in hepatic T cell homeostasis. Upon inhibition of PD-1 signaling, liver CD8$^+$ T cell clones expand and develop key features of chronically activated cells, characterized by the expression of multiple co-inhibitory receptors and 2 transcription factors, TOX and EOMES. These observations are in line with previous reports indicating that in the absence of PD-L1, CD8$^+$ T cells accumulate in the liver of naive and immunized mice.[32,34] Our results strongly suggest that these cells originate from PD-1-expressing liver-resident memory T cells that would otherwise be restrained by physiological PD-1 signaling.[41,54] Unlike other tissues, liver Trms reside within the microvasculature rather than within the stromal epithelium[55] and interact with PD-L1-expressing sinusoidal endothelial cells.[56] As in most other tissue-specific Trms, this liver subset is regulated by the transcription factors Blimp-1, NR4A1, and HOBIT and express low levels of the S1PR1 lymphoid organ retention marker.[49,57,58] Conversely, EOMES down-regulation is required to maintain this specific transcriptional program, as it acts as a direct repressor of HOBIT.[50] PD-1 signaling itself, when TCR priming occurs in the absence of co-stimulation, was shown to inhibit EOMES expression.[59]

Using loss- or gain-of-function strategies, we show here that EOMES plays an additional role in promoting the expansion of liver-resident CD8 T cells and differentiation into Texs. Importantly, this was likely mediated by antigenic stimulation, as we further showed that these expanded cells display an important degree of oligoclonality and did not occur in the absence of antigen persistence.

In the liver, mucosal-associated invariant T (MAIT) and natural killer T (NKT) cells represent a fraction of non-conventional T cells that express high levels of PD-1 and exhibit a more restricted TCR repertoire than classical CD8 T cells.[60,61] They also generally express CD8α monodimers. However, we did not detect the TRAV1-TRAJ33 nor TRAV11-TRAJ18 sequences (characteristic of MAIT and invariant NKT [iNKT] cells, respectively) in the expanded clonotypes that developed upon PD-1 genetic ablation/blockade or transgenic expression of *Eomes*. Moreover, liver PD1$^+$Tox$^+$ cells widely expressed the CD8aβ heterodimer, further supporting the conclusion that exhausted CD8 T cells that accumulate in the liver in the absence of PD-1 signaling most likely develop from conventional Trm CD8 T cells.

It has recently been reported that PD-1 preferentially restrains low-affinity T cell clones.[62] Similarly, EOMES has been shown to be particularly important for the development and maintenance of low-affinity clones during memory T cell formation.[63] It is therefore possible that activation of low-affinity self-reactive clones that have escaped negative thymic selection is controlled in the liver by constitutive PD-1 signaling. Alternatively, liver Trms could also recognize transposable element-encoded retroviral elements expressed by PD-L1$^+$ senescent cells.[64] Hence, it would be useful to evaluate the impact of PD-1 and EOMES on the homeostasis of Trms in aged mice.

Transfer of *in vitro* activated *Pdcd1*$^{-/-}$ CD8 T cells also led to the accumulation of TOX$^+$PD1$^+$ cells in the liver of recipient mice. In this model, Holz et al. showed that antigen presentation within the liver is not mandatory to induce Trm accumulation, although it does promote Trm formation.[65] This experimental setting thus possibly reveals an additional role for PD-1 signaling in controlling the survival of antigen-primed T cells that migrate to the liver and arrive in contact with PDL-1$^+$ sinusoidal endothelial cells.

Of note, 20%–30% of patients under immune checkpoint inhibitors (ICIs) display self-limiting serum aminotransferase

Figure 6. Transgenic expression of EOMES promotes the expansion of liver CD8$^+$ T clones with an exhaustion profile and resident memory features

(A) UMAP plots of 18,675 CD8$^+$ T cells from the spleens and livers of WT and *Eomes*$^{Tg/Tg}$ mice segregated into 15 transcriptional clusters and 11 annotated populations according to their patterns of gene expression.

(B) UMAP plots split by sample and proportions of cells in each annotated population.

(C) UMAP plots showing absolute expression (log-normalized count) of the indicated gene in cells from WT mice or *Eomes*$^{Tg/Tg}$ mice (liver and spleen samples were combined).

(D) Score for the indicated gene signature in each annotated population.

(E) Trajectory analysis using Slingshot. The four lineages are shown together and separately on the UMAP.

See also Figure S10.

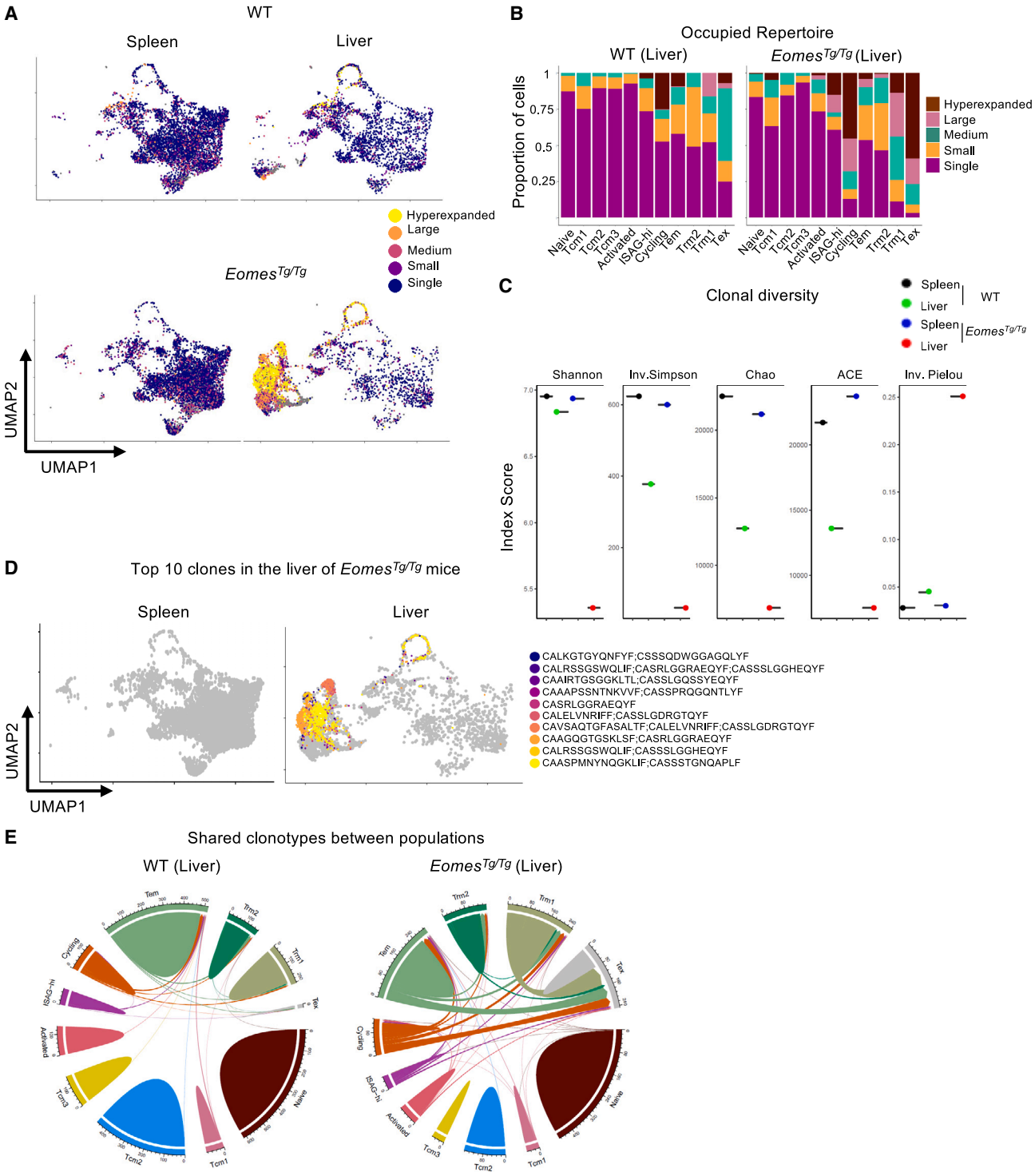

Figure 7. Clonotypic overlap between Trms and Texs in the liver of *Eomes*$^{Tg/Tg}$ mice

(A) UMAP visualization of the clonal size assessed by scTCR-seq of the α and β chains.

(B) The fraction of the repertoire occupied by clonotypes according to their size in each annotated population.

(C) Indices of clonal diversity for each sample.

(D) The 10 most abundant clones identified in the liver of *Eomes*$^{Tg/Tg}$ mice are visualized in the UMAP plots.

(E) Circos plots representing the degree of clonal sharing between populations in the liver of each strain. Each line represents one shared clone.

elevations. Only a minority of patients (1%–2%) develop immune-mediated hepatitis, which is characterized by panlobular hepatitis associated with necrosis and lymphocytic infiltrates of activated $CD8^+$ T cells.[66] It could therefore be of interest to analyze the repertoire and the phenotypic features of these cells upon ICI-induced hepatitis. Recently, 2 studies combining observations in patients with non-alcoholic steatohepatitis (NASH) and murine models also reported the accumulation of liver-resident $CXCR6^+PD\text{-}1^+CD8^+$ T cells.[67,68] This indicates that Trms with exhaustion features could also arise in this pathogenic context; whether this represents non-specific bystander or (self-)antigen-mediated stimulation remains unclear. Importantly, these cells were shown to promote chronic tissular lesions, fibrosis, and hepatocarcinoma development.[67,68]

In conclusion, our results identified an unexpected role for EOMES in PD-1-mediated control of liver Trm homeostasis and could help to better understand the mechanisms involved in immune-related adverse events in patients under ICI.

Limitations of the study

This study has the following limitations.

(1) It remains unclear whether the accumulation of exhausted CD8 T cells is the result of immune events occurring in the liver itself (local expansion and proliferation of a few clones recognizing antigens in the liver that fail to receive PD-1 signaling from liver antigen-presenting cells) or, conversely, is the result of a more systemic effect (T cells migrate to the liver following activation in the absence of PD-1 at extra-hepatic sites). Restricting antigen expression in the liver on hepatocytes should address the contribution of local antigen presentation. Moreover, generation of retrogenic mice (harboring high frequencies of T cells expressing selected clonotypes identified in our study) could also help to evaluate the reactivity of these clonotypes toward liver-specific antigens.

(2) Our study delineates the intrinsic role of EOMES in inducing clonal expansion and acquisition of an exhausted differentiation program in liver $CD8^+$ T cells. Nevertheless, future efforts to understand the role of EOMES in hepatitis infection models would expand our understanding of the biological process. Furthermore, it is possible that *Eomes* overexpression decreases Trm development. Careful analysis of liver Tex differentiation from the Trm progenitor pool could be achieved using Trm fate-mapping mice as previously described in Parga-Vidal et al.[50]

STAR★METHODS

Detailed methods are provided in the online version of this paper and include the following:

- KEY RESOURCES TABLE
- RESOURCE AVAILABILITY
  - Lead contact
  - Materials availability
  - Data and code availability
- EXPERIMENTAL MODEL AND STUDY PARTICIPANT DETAILS
- METHOD DETAILS
  - Cell preparation
  - Flow cytometry staining
  - Cell cultures and *ex vivo* stimulations
  - Adoptive transfer experiment
  - Anti-PD-1 treatment
  - Gini TCR skewing index
  - L. monocytogenes infection
  - Cell sorting
  - Bulk TCR-sequencing
  - ATAC-sequencing
  - scRNA-sequencing and scTCR-sequencing
- QUANTIFICATION AND STATISTICAL ANALYSIS

SUPPLEMENTAL INFORMATION

Supplemental information can be found online at https://doi.org/10.1016/j.celrep.2023.112876.

ACKNOWLEDGMENTS

The authors wish to thank Guillaume Oldenhove, Kevin Englebert, Vincent Martens, Nicolas Istaces, Oberdan Leo, and Veronique Flamand and her team for sharing critical reagents, for providing technical help, or for useful discussions. This study was supported by the Fonds National de la Recherche Scientifique (FRS-FNRS, Belgium), the European Regional Development Fund (ERDF) of the Walloon Region (Wallonia-Biomed portfolio, 411132-957270), and the Fonds Erasme (Erasme Hospital, Université Libre de Bruxelles). M.L.M. and G.S.S. are research fellows, F.A. is a research associate, and S.G. is a research director of the FRS-FNRS.

AUTHOR CONTRIBUTIONS

M.L.M. conducted most of the experiments. A.A., G.S.S., S. Dejolier, M.N., S.T., V.S., H.D., and S. Denanglaire contributed to some experiments. A.A., G.S.S., and F.L. performed bioinformatics analysis. M.L.M., A.A., G.S.S., and S. Dejolier analyzed the data and prepared the figures. D.V. and F.A. provided input for data analysis and interpretation. F.A. supervised reviewing experiments and analysis. M.L.M., F.A., and S.G. wrote the manuscript. S.G. supervised the work. All authors were involved in critically revising the manuscript for important intellectual content. All authors had full access to the data and approved the manuscript before it was submitted by the corresponding author.

DECLARATION OF INTERESTS

The authors declare no competing interests.

INCLUSION AND DIVERSITY

We support inclusive, diverse, and equitable conduct of research.

Received: November 30, 2022
Revised: June 2, 2023
Accepted: July 11, 2023
Published: August 4, 2023

REFERENCES

1. Brahmer, J.R., Tykodi, S.S., Chow, L.Q.M., Hwu, W.J., Topalian, S.L., Hwu, P., Drake, C.G., Camacho, L.H., Kauh, J., Odunsi, K., et al. (2012).

Safety and activity of anti-PD-L1 antibody in patients with advanced cancer. N. Engl. J. Med. *366*, 2455–2465.

2. Ribas, A., and Wolchok, J.D. (2018). Cancer immunotherapy using checkpoint blockade. Science *359*, 1350–1355.
3. Hashimoto, M., Kamphorst, A.O., Im, S.J., Kissick, H.T., Pillai, R.N., Ramalingam, S.S., Araki, K., and Ahmed, R. (2018). CD8 T cell exhaustion in chronic infection and cancer: opportunities for interventions. Annu. Rev. Med. *69*, 301–318.
4. Chikuma, S., Terawaki, S., Hayashi, T., Nabeshima, R., Yoshida, T., Shibayama, S., Okazaki, T., and Honjo, T. (2009). PD-1-mediated suppression of IL-2 production induces CD8+ T cell anergy in vivo. J. Immunol. *182*, 6682–6689.
5. Ahn, E., Araki, K., Hashimoto, M., Li, W., Riley, J.L., Cheung, J., Sharpe, A.H., Freeman, G.J., Irving, B.A., and Ahmed, R. (2018). Role of PD-1 during effector CD8 T cell differentiation. Proc. Natl. Acad. Sci. USA *115*, 4749–4754.
6. Barber, D.L., Wherry, E.J., Masopust, D., Zhu, B., Allison, J.P., Sharpe, A.H., Freeman, G.J., and Ahmed, R. (2006). Restoring function in exhausted CD8 T cells during chronic viral infection. Nature *439*, 682–687.
7. Oestreich, K.J., Yoon, H., Ahmed, R., and Boss, J.M. (2008). NFATc1 regulates programmed death-1 expression upon T cell activation. J. Immunol. *181*, 4832–4839.
8. Martinez, G.J., Pereira, R.M., Äijö, T., Kim, E.Y., Marangoni, F., Pipkin, M.E., Togher, S., Heissmeyer, V., Zhang, Y.C., Crotty, S., et al. (2015). The transcription factor NFAT promotes exhaustion of activated CD8+ T cells. Immunity *42*, 265–278.
9. Philip, M., and Schietinger, A. (2022). CD8+ T cell differentiation and dysfunction in cancer. Nat. Rev. Immunol. *22*, 209–223.
10. Alfei, F., Kanev, K., Hofmann, M., Wu, M., Ghoneim, H.E., Roelli, P., Utzschneider, D.T., von Hoesslin, M., Cullen, J.G., Fan, Y., et al. (2019). TOX reinforces the phenotype and longevity of exhausted T cells in chronic viral infection. Nature *571*, 265–269.
11. Khan, O., Giles, J.R., McDonald, S., Manne, S., Ngiow, S.F., Patel, K.P., Werner, M.T., Huang, A.C., Alexander, K.A., Wu, J.E., et al. (2019). TOX transcriptionally and epigenetically programs CD8+ T cell exhaustion. Nature *571*, 211–218.
12. Scott, A.C., Dündar, F., Zumbo, P., Chandran, S.S., Klebanoff, C.A., Shakiba, M., Trivedi, P., Menocal, L., Appleby, H., Camara, S., et al. (2019). TOX is a critical regulator of tumour-specific T cell differentiation. Nature *571*, 270–274.
13. Yao, C., Sun, H.W., Lacey, N.E., Ji, Y., Moseman, E.A., Shih, H.Y., Heuston, E.F., Kirby, M., Anderson, S., Cheng, J., et al. (2019). Single-cell RNA-seq reveals TOX as a key regulator of CD8+ T cell persistence in chronic infection. Nat. Immunol. *20*, 890–901.
14. Seo, H., Chen, J., González-Avalos, E., Samaniego-Castruita, D., Das, A., Wang, Y.H., López-Moyado, I.F., Georges, R.O., Zhang, W., Onodera, A., et al. (2019). TOX and TOX2 transcription factors cooperate with NR4A transcription factors to impose CD8+ T cell exhaustion. Proc. Natl. Acad. Sci. USA *116*, 12410–12415.
15. Zhou, X., Yu, S., Zhao, D.M., Harty, J.T., Badovinac, V.P., and Xue, H.H. (2010). Differentiation and persistence of memory CD8+ T cells depend on T cell factor 1. Immunity *33*, 229–240.
16. Im, S.J., Hashimoto, M., Gerner, M.Y., Lee, J., Kissick, H.T., Burger, M.C., Shan, Q., Hale, J.S., Lee, J., Nasti, T.H., et al. (2016). Defining CD8+ T cells that provide the proliferative burst after PD-1 therapy. Nature *537*, 417–421.
17. Utzschneider, D.T., Charmoy, M., Chennupati, V., Pousse, L., Ferreira, D.P., Calderon-Copete, S., Danilo, M., Alfei, F., Hofmann, M., Wieland, D., et al. (2016). T cell factor 1-expressing memory-like CD8(+) T cells sustain the immune response to chronic viral infections. Immunity *45*, 415–427.
18. Miller, B.C., Sen, D.R., Al Abosy, R., Bi, K., Virkud, Y.V., LaFleur, M.W., Yates, K.B., Lako, A., Felt, K., Naik, G.S., et al. (2019). Subsets of exhausted CD8+ T cells differentially mediate tumor control and respond to checkpoint blockade. Nat. Immunol. *20*, 326–336.
19. Paley, M.A., Kroy, D.C., Odorizzi, P.M., Johnnidis, J.B., Dolfi, D.V., Barnett, B.E., Bikoff, E.K., Robertson, E.J., Lauer, G.M., Reiner, S.L., and Wherry, E.J. (2012). Progenitor and terminal subsets of CD8+ T cells cooperate to contain chronic viral infection. Science *338*, 1220–1225.
20. Beltra, J.-C., Manne, S., Abdel-Hakeem, M.S., Kurachi, M., Giles, J.R., Chen, Z., Casella, V., Ngiow, S.F., Khan, O., Huang, Y.J., et al. (2020). Developmental relationships of four exhausted CD8+ T cell subsets reveals underlying transcriptional and epigenetic landscape control mechanisms. Immunity *52*, 825–841.e8.
21. Li, J., He, Y., Hao, J., Ni, L., and Dong, C. (2018). High levels of eomes promote exhaustion of anti-tumor CD8+ T cells. Front. Immunol. *9*, 2981.
22. Riaz, N., Havel, J.J., Makarov, V., Desrichard, A., Urba, W.J., Sims, J.S., Hodi, F.S., Martín-Algarra, S., Mandal, R., Sharfman, W.H., et al. (2017). Tumor and microenvironment evolution during immunotherapy with nivolumab. Cell *171*, 934–949.e16.
23. Tumeh, P.C., Harview, C.L., Yearley, J.H., Shintaku, I.P., Taylor, E.J.M., Robert, L., Chmielowski, B., Spasic, M., Henry, G., Ciobanu, V., et al. (2014). PD-1 blockade induces responses by inhibiting adaptive immune resistance. Nature *515*, 568–571.
24. Kato, T., Kiyotani, K., Tomiyama, E., Koh, Y., Matsushita, M., Hayashi, Y., Nakano, K., Ishizuya, Y., Wang, C., Hatano, K., et al. (2021). Peripheral T cell receptor repertoire features predict durable responses to anti-PD-1 inhibitor monotherapy in advanced renal cell carcinoma. Oncoimmunology *10*, 1862948.
25. Roh, W., Chen, P.L., Reuben, A., Spencer, C.N., Prieto, P.A., Miller, J.P., Gopalakrishnan, V., Wang, F., Cooper, Z.A., Reddy, S.M., et al. (2017). Integrated molecular analysis of tumor biopsies on sequential CTLA-4 and PD-1 blockade reveals markers of response and resistance. Sci. Transl. Med. *9*, eaah3560.
26. Amaria, R.N., Reddy, S.M., Tawbi, H.A., Davies, M.A., Ross, M.I., Glitza, I.C., Cormier, J.N., Lewis, C., Hwu, W.J., Hanna, E., et al. (2018). Neoadjuvant immune checkpoint blockade in high-risk resectable melanoma. Nat. Med. *24*, 1649–1654.
27. Wu, T.D., Madireddi, S., de Almeida, P.E., Banchereau, R., Chen, Y.J.J., Chitre, A.S., Chiang, E.Y., Iftikhar, H., O'Gorman, W.E., Au-Yeung, A., et al. (2020). Peripheral T cell expansion predicts tumour infiltration and clinical response. Nature *579*, 274–278.
28. Postow, M.A., Sidlow, R., and Hellmann, M.D. (2018). Immune-related adverse events associated with immune checkpoint blockade. N. Engl. J. Med. *378*, 158–168.
29. Michot, J.M., Bigenwald, C., Champiat, S., Collins, M., Carbonnel, F., Postel-Vinay, S., Berdelou, A., Varga, A., Bahleda, R., Hollebecque, A., et al. (2016). Immune-related adverse events with immune checkpoint blockade: a comprehensive review. Eur. J. Cancer *54*, 139–148.
30. Nishimura, H., Nose, M., Hiai, H., Minato, N., and Honjo, T. (1999). Development of lupus-like autoimmune diseases by disruption of the PD-1 gene encoding an ITIM motif-carrying immunoreceptor. Immunity *11*, 141–151.
31. Nishimura, H., Okazaki, T., Tanaka, Y., Nakatani, K., Hara, M., Matsumori, A., Sasayama, S., Mizoguchi, A., Hiai, H., Minato, N., and Honjo, T. (2001). Autoimmune dilated cardiomyopathy in PD-1 receptor-deficient mice. Science *291*, 319–322.
32. Dong, H., Zhu, G., Tamada, K., Flies, D.B., van Deursen, J.M.A., and Chen, L. (2004). B7-H1 determines accumulation and deletion of intrahepatic CD8(+) T lymphocytes. Immunity *20*, 327–336.
33. Odorizzi, P.M., Pauken, K.E., Paley, M.A., Sharpe, A., and Wherry, E.J. (2015). Genetic absence of PD-1 promotes accumulation of terminally differentiated exhausted CD8+ T cells. J. Exp. Med. *212*, 1125–1137.
34. Charlton, J.J., Chatzidakis, I., Tsoukatou, D., Boumpas, D.T., Garinis, G.A., and Mamalaki, C. (2013). Programmed death-1 shapes memory phenotype CD8 T cell subsets in a cell-intrinsic manner. J. Immunol. *190*, 6104–6114.

35. Pauken, K.E., Godec, J., Odorizzi, P.M., Brown, K.E., Yates, K.B., Ngiow, S.F., Burke, K.P., Maleri, S., Grande, S.M., Francisco, L.M., et al. (2020). The PD-1 pathway regulates development and function of memory CD8+ T cells following respiratory viral infection. Cell Rep. *31*, 107827.

36. Joshi, N.S., Cui, W., Chandele, A., Lee, H.K., Urso, D.R., Hagman, J., Gapin, L., and Kaech, S.M. (2007). Inflammation directs memory precursor and short-lived effector CD8(+) T cell fates via the graded expression of T-bet transcription factor. Immunity *27*, 281–295.

37. Kaech, S.M., Tan, J.T., Wherry, E.J., Konieczny, B.T., Surh, C.D., and Ahmed, R. (2003). Selective expression of the interleukin 7 receptor identifies effector CD8 T cells that give rise to long-lived memory cells. Nat. Immunol. *4*, 1191–1198.

38. Fernandez-Ruiz, D., Ng, W.Y., Holz, L.E., Ma, J.Z., Zaid, A., Wong, Y.C., Lau, L.S., Mollard, V., Cozijnsen, A., Collins, N., et al. (2016). Liver-resident memory CD8+ T cells form a front-line defense against malaria liver-stage infection. Immunity *45*, 889–902.

39. Tse, S.-W., Radtke, A.J., Espinosa, D.A., Cockburn, I.A., and Zavala, F. (2014). The Chemokine receptor CXCR6 is required for the maintenance of liver memory CD8+ T cells specific for infectious pathogens. J. Infect. Dis. *210*, 1508–1516.

40. Ray, S.J., Franki, S.N., Pierce, R.H., Dimitrova, S., Kotliansky, V., Sprague, A.G., Doherty, P.C., de Fougerolles, A.R., and Topham, D.J. (2004). The collagen binding alpha1beta1 integrin VLA-1 regulates CD8 T cell-mediated immune protection against heterologous influenza infection. Immunity *20*, 167–179.

41. Kim, J.H., Han, J.W., Choi, Y.J., Rha, M.S., Koh, J.Y., Kim, K.H., Kim, C.G., Lee, Y.J., Kim, A.R., Park, J., et al. (2020). Functions of human liver CD69+CD103-CD8+ T cells depend on HIF-2α activity in healthy and pathologic livers. J. Hepatol. *72*, 1170–1181.

42. van der Geest, K.S.M., Abdulahad, W.H., Horst, G., Lorencetti, P.G., Bijzet, J., Arends, S., van der Heiden, M., Buisman, A.M., Kroesen, B.J., Brouwer, E., and Boots, A.M.H. (2015). Quantifying distribution of flow cytometric TCR-Vβ usage with economic statistics. PLoS One *10*, e0125373.

43. Wang, N., Strugnell, R.A., Wijburg, O.L., and Brodnicki, T.C. (2013). Systemic infection of Mice with Listeria monocytogenes to characterize host immune responses. Methods Mol. Biol. *1031*, 125–144.

44. Cheers, C., and McKenzie, I.F. (1978). Resistance and susceptibility of mice to bacterial infection: genetics of listeriosis. Infect. Immun. *19*, 755–762.

45. Pritykin, Y., van der Veeken, J., Pine, A.R., Zhong, Y., Sahin, M., Mazutis, L., Pe'er, D., Rudensky, A.Y., and Leslie, C.S. (2021). A unified atlas of CD8 T cell dysfunctional states in cancer and infection. Mol. Cell *81*, 2477–2493.e10.

46. Crowl, J.T., Heeg, M., Ferry, A., Milner, J.J., Omilusik, K.D., Toma, C., He, Z., Chang, J.T., and Goldrath, A.W. (2022). Tissue-resident memory CD8+ T cells possess unique transcriptional, epigenetic and functional adaptations to different tissue environments. Nat. Immunol. *23*, 1121–1131. https://doi.org/10.1038/s41590-022-01229-8.

47. van der Veeken, J., Zhong, Y., Sharma, R., Mazutis, L., Dao, P., Pe'er, D., Leslie, C.S., and Rudensky, A.Y. (2019). Natural genetic variation reveals key features of epigenetic and transcriptional memory in virus-specific CD8 T cells. Immunity *50*, 1202–1217.e7.

48. Intlekofer, A.M., Takemoto, N., Wherry, E.J., Longworth, S.A., Northrup, J.T., Palanivel, V.R., Mullen, A.C., Gasink, C.R., Kaech, S.M., Miller, J.D., et al. (2005). Effector and memory CD8+ T cell fate coupled by T-bet and eomesodermin. Nat. Immunol. *6*, 1236–1244.

49. Mackay, L.K., Minnich, M., Kragten, N.A.M., Liao, Y., Nota, B., Seillet, C., Zaid, A., Man, K., Preston, S., Freestone, D., et al. (2016). Hobit and Blimp1 instruct a universal transcriptional program of tissue residency in lymphocytes. Science *352*, 459–463.

50. Parga-Vidal, L., Behr, F.M., Kragten, N.A.M., Nota, B., Wesselink, T.H., Kavazović, I., Covill, L.E., Schuller, M.B.P., Bryceson, Y.T., Wensveen, F.M., et al. (2021). Hobit identifies tissue-resident memory T cell precursors that are regulated by Eomes. Sci. Immunol. *6*, eabg3533.

51. Carmona, S.J., Siddiqui, I., Bilous, M., Held, W., and Gfeller, D. (2020). Deciphering the transcriptomic landscape of tumor-infiltrating CD8 lymphocytes in B16 melanoma tumors with single-cell RNA-Seq. Oncoimmunology *9*, 1737369.

52. Koda, Y., Teratani, T., Chu, P.S., Hagihara, Y., Mikami, Y., Harada, Y., Tsujikawa, H., Miyamoto, K., Suzuki, T., Taniki, N., et al. (2021). CD8+ tissue-resident memory T cells promote liver fibrosis resolution by inducing apoptosis of hepatic stellate cells. Nat. Commun. *12*, 4474.

53. Street, K., Risso, D., Fletcher, R.B., Das, D., Ngai, J., Yosef, N., Purdom, E., and Dudoit, S. (2018). Slingshot: cell lineage and pseudotime inference for single-cell transcriptomics. BMC Genom. *19*, 477.

54. Pallett, L.J., Davies, J., Colbeck, E.J., Robertson, F., Hansi, N., Easom, N.J.W., Burton, A.R., Stegmann, K.A., Schurich, A., Swadling, L., et al. (2017). IL-2high tissue-resident T cells in the human liver: sentinels for hepatotropic infection. J. Exp. Med. *214*, 1567–1580.

55. Pallett, L.J., and Maini, M.K. (2022). Liver-resident memory T cells: life in lockdown. Semin. Immunopathol. *44*, 813–825. https://doi.org/10.1007/s00281-022-00932-w.

56. Horst, A.K., Neumann, K., Diehl, L., and Tiegs, G. (2016). Modulation of liver tolerance by conventional and nonconventional antigen-presenting cells and regulatory immune cells. Cell. Mol. Immunol. *13*, 277–292.

57. Boddupalli, C.S., Nair, S., Gray, S.M., Nowyhed, H.N., Verma, R., Gibson, J.A., Abraham, C., Narayan, D., Vasquez, J., Hedrick, C.C., et al. (2016). ABC transporters and NR4A1 identify a quiescent subset of tissue-resident memory T cells. J. Clin. Invest. *126*, 3905–3916.

58. Skon, C.N., Lee, J.Y., Anderson, K.G., Masopust, D., Hogquist, K.A., and Jameson, S.C. (2013). Transcriptional downregulation of S1pr1 is required for the establishment of resident memory CD8+ T cells. Nat. Immunol. *14*, 1285–1293.

59. Nurieva, R., Thomas, S., Nguyen, T., Martin-Orozco, N., Wang, Y., Kaja, M.K., Yu, X.Z., and Dong, C. (2006). T-cell tolerance or function is determined by combinatorial costimulatory signals. EMBO J. *25*, 2623–2633.

60. Rahimpour, A., Koay, H.F., Enders, A., Clanchy, R., Eckle, S.B.G., Meehan, B., Chen, Z., Whittle, B., Liu, L., Fairlie, D.P., et al. (2015). Identification of phenotypically and functionally heterogeneous mouse mucosal-associated invariant T cells using MR1 tetramers. J. Exp. Med. *212*, 1095–1108.

61. Benlagha, K., Weiss, A., Beavis, A., Teyton, L., and Bendelac, A. (2000). In vivo identification of glycolipid antigen-specific T cells using fluorescent CD1d tetramers. J. Exp. Med. *191*, 1895–1903.

62. Shimizu, K., Sugiura, D., Okazaki, I.M., Maruhashi, T., Takemoto, T., and Okazaki, T. (2021). PD-1 preferentially inhibits the activation of low-affinity T cells. Proc. Natl. Acad. Sci. USA *118*, e2107141118.

63. Kavazović, I., Han, H., Balzaretti, G., Slinger, E., Lemmermann, N.A.W., Ten Brinke, A., Merkler, D., Koster, J., Bryceson, Y.T., de Vries, N., et al. (2020). Eomes broadens the scope of CD8 T-cell memory by inhibiting apoptosis in cells of low affinity. PLoS Biol. *18*, e3000648.

64. Wang, T.-W., Johmura, Y., Suzuki, N., Omori, S., Migita, T., Yamaguchi, K., Hatakeyama, S., Yamazaki, S., Shimizu, E., Imoto, S., et al. (2022). Blocking PD-L1–PD-1 improves senescence surveillance and ageing phenotypes. Nature *611*, 358–364.

65. Holz, L.E., Prier, J.E., Freestone, D., Steiner, T.M., English, K., Johnson, D.N., Mollard, V., Cozijnsen, A., Davey, G.M., Godfrey, D.I., et al. (2018). CD8+ T cell activation leads to constitutive formation of liver tissue-resident memory T cells that seed a large and flexible niche in the liver. Cell Rep. *25*, 68–79.e4.

66. De Martin, E., Michot, J.M., Papouin, B., Champiat, S., Mateus, C., Lambotte, O., Roche, B., Antonini, T.M., Coilly, A., Laghouati, S., et al. (2018). Characterization of liver injury induced by cancer immunotherapy using immune checkpoint inhibitors. J. Hepatol. *68*, 1181–1190.

67. Dudek, M., Pfister, D., Donakonda, S., Filpe, P., Schneider, A., Laschinger, M., Hartmann, D., Hüser, N., Meiser, P., Bayerl, F., et al. (2021). Auto-aggressive CXCR6+ CD8 T cells cause liver immune pathology in NASH. Nature *592*, 444–449.

68. Pfister, D., Núñez, N.G., Pinyol, R., Govaere, O., Pinter, M., Szydlowska, M., Gupta, R., Qiu, M., Deczkowska, A., Weiner, A., et al. (2021). NASH limits anti-tumour surveillance in immunotherapy-treated HCC. Nature *592*, 450–456.

69. Foulds, K.E., Zenewicz, L.A., Shedlock, D.J., Jiang, J., Troy, A.E., and Shen, H. (2002). Cutting edge: CD4 and CD8 T cells are intrinsically different in their proliferative responses. J. Immunol. *168*, 1528–1532.

70. Istaces, N., Splittgerber, M., Lima Silva, V., Nguyen, M., Thomas, S., Le, A., Achouri, Y., Calonne, E., Defrance, M., Fuks, F., et al. (2019). EOMES interacts with RUNX3 and BRG1 to promote innate memory cell formation through epigenetic reprogramming. Nat. Commun. *10*, 3306.

71. Bolotin, D.A., Poslavsky, S., Mitrophanov, I., Shugay, M., Mamedov, I.Z., Putintseva, E.V., and Chudakov, D.M. (2015). MiXCR: software for comprehensive adaptive immunity profiling. Nat. Methods *12*, 380–381.

72. Shugay, M., Bagaev, D.V., Turchaninova, M.A., Bolotin, D.A., Britanova, O.V., Putintseva, E.V., Pogorelyy, M.V., Nazarov, V.I., Zvyagin, I.V., Kirgizova, V.I., et al. (2015). VDJtools: unifying Post-analysis of T Cell Receptor Repertoires. PLoS Comput. Biol. *11*, e1004503.

73. ImmunoMind Team. Immunarch (2019). An R Package for Painless Bioinformatics Analysis of T-Cell and B-Cell Immune Repertoires. Zenodo. https://doi.org/10.5281/zenodo.3367200.

74. Ramírez, F., Ryan, D.P., Gruning, B., Bhardwaj, V., Kilpert, F., Richter, A.S., Heyne, S., Dundar, F., and Manke, T. (2016). deepTools2: a next generation web server for deep-sequencing data analysis. Nucleic Acids Research *257*.

75. Stuart, T., Butler, A., Hoffman, P., Hafemeister, C., Papalexi, E., Mauck, W.M., 3rd, Hao, Y., Stoeckius, M., Smibert, P., and Satija, R. (2019). Comprehensive integration of single-cell data. Cell *177*, 1888–1902.e21.

76. Cao, J., Spielmann, M., Qiu, X., Huang, X., Ibrahim, D.M., Hill, A.J., Zhang, F., Mundlos, S., Christiansen, L., Steemers, F.J., et al. (2019). The single-cell transcriptional landscape of mammalian organogenesis. Nature *566*, 496–502.

77. Borcherding, N., Bormann, N.L., and Kraus, G. (2020). scRepertoire: An R-based toolkit for single-cell immune receptor analysis. F1000Res *9*, 47.

78. Gu, Z., Gu, L., Eils, R., Schlesner, M., and Brors, B. (2014). Circlize implements and enhances circular visualization in R. Bioinformatics *30*, 2811–2812.

79. Van Caeneghem, Y., De Munter, S., Tieppo, P., Goetgeluk, G., Weening, K., Verstichel, G., Bonte, S., Taghon, T., Leclercq, G., Kerre, T., et al. (2017). Antigen receptor-redirected T cells derived from hematopoietic precursor cells lack expression of the endogenous TCR/CD3 receptor and exhibit specific antitumor capacities. Oncoimmunology *6*, e1283460.

80. Bioinformatics Analysis of T-Cell and B-Cell Immune Repertoires. https://immunarch.com/.

81. McLean, C.Y., Bristor, D., Hiller, M., Clarke, S.L., Schaar, B.T., Lowe, C.B., Wenger, A.M., and Bejerano, G. (2010). GREAT improves functional interpretation of cis-regulatory regions. Nat. Biotechnol. *28*, 495–501.

82. Gearing, L.J., Cumming, H.E., Chapman, R., Finkel, A.M., Woodhouse, I.B., Luu, K., Gould, J.A., Forster, S.C., and Hertzog, P.J. (2019). CiiiDER: a tool for predicting and analysing transcription factor binding sites. PLoS One *14*, e0215495.

STAR★METHODS

KEY RESOURCES TABLE

REAGENT or RESOURCE	SOURCE	IDENTIFIER
Antibodies		
BV711 Hamster anti-mouse CD3e; clone 145-2C11; 1:100	BD Biosciences	Cat# 563123; RRID: AB_2687954
AF700 rat anti-mouse CD4; clone RM4-5; 1:100	BD Biosciences	Cat# 561025; RRID: AB_396956
APC-Cy7 rat anti-mouse CD4; clone RM4-5; 1:100	BD Biosciences	Cat# 565650; RRID: AB_2739324
PE-Cy7 rat anti-mouse CD4; clone RM4-5; 1:100	BD Biosciences	Cat# 561099; RRID: AB_394461
PerCP rat anti-mouse CD8a; clone 53–6.7; 1:50	BD Biosciences	Cat# 561092; RRID: AB_394573
BV510 rat anti-mouse CD8a; clone 53–6.7; 1:50	BD Biosciences	Cat# 563068; RRID: AB_2687548
PE-Cy7 Hamster anti-mouse CD11c; clone HL3; 1:100	BD Biosciences	Cat# 561022; RRID: AB_647251
PE-Cy7 rat anti-mouse CD19; clone 1D3; 1:100	BD Biosciences	Cat# 557655; RRID: AB_396770
FITC rat anti-mouse CD44; clone IM7; 1:50	BD Biosciences	Cat# 561859; RRDI: AB_2076224
V450 rat anti-mouse CD44; clone IM7; 1:50	BD Biosciences	Cat# 560451; RRID: AB_1645273
BUV395 rat anti-mouse CD44; clone IM7; 1:50	BD Biosciences	Cat# 740215; RRID: AB_2739963
BUV496 rat anti-mouse; CD44; clone IM7; 1:50	BD Biosciences	Cat# 741057; RRID: AB_2870671
BV650 rat anti-mouse CD49d; clone R1-2; 1:50	BD Biosciences	Cat# 740458; RRID: AB_2740185
BV786 rat anti-mouse CD62L; clone MEL-14; 1:100	BD Biosciences	Cat# 564109; RRID: AB_2738598
FITC rat anti-mouse CD62L; clone MEL-14; 1:100	BD Biosciences	Cat# 553150; RRID: AB_394665
BUV 737 Hamster anti-mouse CD69; clone H1.2F3; 1:100	BD Biosciences	Cat# 612793; RRID:AB_2870120
BV711 rat anti-mouse CD103; clone M290; 1:100	BD Biosciences	Cat# 564320; RRID: AB_2738743
BV421 rat anti-mouse CD127; clone SB/199; 1:100	BD Biosciences	Cat# 562959; RRID: AB_2737917
PE-Cy7 rat anti-mouse CD127; clone SB/199; 1:50	BD Biosciences	Cat# 560733; RRID: AB_1727424
AF647 mouse anti-Human GZMB; clone GB11; 1:100	BD Biosciences	Cat# 560212; RRID: AB_11154033
BV786 rat anti-mouse IFNg; cloneXMG1.2; 1:100	BD Biosciences	Cat# 563773; RRID: AB_2738419
AF700 mouse anti- Ki-67; clone B56; 1:50	BD Biosciences	Cat# 561277; RRID:AB_10611571
AF700 Hamster anti-mouse TCRb chain; clone H57-597; 1:100	BD Biosciences	Cat# 560705; RRID: AB_1727573
FITC Hamster anti-mouse TCRb chain; clone H57-597, 1:100	BD Biosciences	Cat# 553170; RRID: AB_394683

(*Continued on next page*)

Continued

REAGENT or RESOURCE	SOURCE	IDENTIFIER
PerCP-Cy5.5 Hamster anti-mouse TCRb chain; clone H57-597; 1:100	BD Biosciences	Cat# 560657; RRID: AB_1727575
APC Hamster anti-mouse KLRG-1; clone 2F1; 1:100	BD Biosciences	Cat# 561620; RRID:AB_10895798
BV650 Hamster Anti-Rat/Mouse CD49a; clone Ha31/8; 1:100	BD Biosciences	Cat# 740519; RRID:AB_2740235
PE mouse- anti-TCF-7/TCF-1; clone S33-966; 1:50	BD Biosciences	Cat# 564217; RRID:AB_2687845
BV421 rat anti-mouse CD38; clone 90/CD38; 1:25	BD Biosciences	Cat# 562768; RRID:AB_2737781
BV650 mouse anti-mouse TIGIT; clone 1G9; 1:100	BD Biosciences	Cat# 744213; RRID: AB_2742062
BV786 mouse anti-mouse CD366 (TIM-3); clone 5D12/TIM-3; 1:100	BD Biosciences	Cat# 747621; RRID: AB_2744187
PerCP-Cy™5.5 rat anti-mouse CD223 (Lag3); clone C9B7W; 1:100	BD Biosciences	Cat# 564673; RRID: AB_2734764
BV711 mouse anti-mouse CD244.2; clone 2B4; 1:100	BD Biosciences	Cat#740671; RRID: AB_2740359
PE-CF594 Hamster anti-mouse CD279 (PD-1); clone J43; 1:100	BD Biosciences	Cat#562523; RRID: AB_2737634
PE rat anti-mouse CD4; clone RM4-5; 1:100	BD Biosciences	Cat#553049; RRID: AB_394585
eFluor™ 660 EOMES; clone Dan11mag; 1:75	eBioscience	Cat#50-4875-82; RRID AB_2574227
PE EOMES; clone Dan11mag; 1:75	eBioscience	Cat#12-4875-82; RRID AB_1603275
PE-Cy7 EOMES; clone Dan11mag; 1:75	eBioscience	Cat#25-4875-82; RRID AB_11042699
PE-Cy7 T-bet; clone eBio4B10 (4B10); 1:75	eBioscience	Cat#25-5825-82; RRID AB_11042699
eF660 TOX; clone TXRX10; 1:100	eBioscience	Cat#50-6502-82; RRID AB_2574265
Super Bright™436 CD39; clone 24DMS1: 1:200	eBioscience	Cat#62-0391-82; RRID AB_2637139
BV421 CD186 (CXCR6); clone SA051D1; 1:100	Biolegend	Cat#62-0391-82; RRID AB_ 2616760
AF700 rat anti-mouse CD45, clone 30-F11 (RUO) 1:100	BD Biosciences	Cat#560510; RRID AB_1645208
BUV395 rat anti-mouse CD45, clone 30-F11 (RUO) 1:100	BD Biosciences	Cat#564279; RRID AB_2651134
AF700 rat anti-mouse CD45.2, clone 104 (RUO) 1:100	BD Biosciences	Cat#560693; RRID AB_1727491
BUV395 rat anti-mouse CD45.1, clone A20 (RUO) 1:100	BD Biosciences	Cat#565212; RRID AB_2722493
Anti-mouse TCR VB screening panel	BD Biosciences	Cat#557004; RRID: AB_647180
H-2Kb/SIINFEKL tetramer conjugated to phycoerythrin (PE)	ProImmune	Cat#F093; RRID: N/A
ViaKrome 808 Fixable Viability Dye	Beckman Coulter	Cat#C36628; RRID: N/A
LIVE/DEAD™ Fixable Aqua dead cell stain kit, for 405 nm excitation	Invitrogen	Cat#L34957; RRID: N/A

(*Continued on next page*)

Continued

REAGENT or RESOURCE	SOURCE	IDENTIFIER
LIVE/DEAD™ Fixable Near-IR dead cell stain kit, for 633 or 635 nm excitation	Invitrogen	Cat# L10119; RRID: N/A
Purified rat anti-mouse CD16/CD32; clone 2.4G2; 1:100	BD Biosciences	Cat#553141; RRID: AB_394656
EBioscience™ Foxp3/Transcription factor staining buffer set	Life Technologies	Cat#00-5523-00; RRID: N/A
InVivoMAb anti-mouse anti-PD-1 clone RPM1-14 200μg/mice	BioXcell	Cat#BE0146; RRID: AB_10949053
InVivoMAb anti-mouse CD28 (1μg/mL) clone:D665	BioXcell	Cat#BE0328; RRID: AB_2819055
InVivoMAb anti-mouse CD3 (1μg/mL) clone:17A2	BioXcell	Cat#BE0002; RRID: AB_1107630
TotalSeq™-C0302 anti-mouse hashtag 2 antibody	Biolegend	Cat#155863; RRID: AB_2800694
TotalSeq™-C 0303 anti-mouse hashtag 3 antibody	Biolegend	Cat#155865; RRID: AB_2800695
TotalSeq™-C 0304 anti-mouse hashtag 4 antibody	Biolegend	Cat#155867; RRID: AB_2800696
TotalSeq™-C 0305 anti-mouse hashtag 5 antibody	Biolegend	Cat#155869; RRID: AB_2800697
TotalSeq™-C 0306 anti-mouse hashtag 6 antibody	Biolegend	Cat#155871; RRID: AB_2819910
TotalSeq™-C 0307 anti-mouse hashtag 7 antibody	Biolegend	Cat#155873; RRID: AB_2819910
Bacterial and virus strains		
Attenuated Listeria monocytogenes strain expressing OVA (Δ*actA* rLmOVA)	Provided by Dr Hao Shen (Foulds et al.)[69]	N/A
Chemicals, peptides, and recombinant proteins		
Phorbol 12-mystrate 13-acetate; 50 ng/mL	Sigma	Cat#79346; CAS n°:16561-29-8
Ionomycin calcium salt; 1μg/mL	Sigma	Cat#I3909; RRID: N/A
Recombinant human IL-2 (10 ng/mL)	Bio-Techne	Cat# 202-IL/CF; RRID: N/A
Critical commercial assays		
Dynabeads Untouched mouse CD8 cells kit	Life Technologies	Cat#11417D; RRID: N/A
RNeasy Micro kit	Qiagen	Cat#217084; RRID: N/A
PaxGene blood RNA kit	Qiagen	Cat#762164; RRID: N/A
Nextera DNA sample prep kit	Illumina	Cat#FC-121-1031; RRID: N/A
MinElute PCR purification kit	Qiagen	Cat#28004; RRID: N/A
Bioanalyzer high-Sensitivity DNA analysis kit	Agilent	Cat #5067-4626; RRID: N/A
NEBNext high Fidelity 2xPCR Master mix	New England Biolabs	Cat#M0541S; RRID: N/A
Chromium single cell 5′V1.1 reagent kit	10x Genomics	PN-1000020; RRID: N/A
Chromium single cell 5′ reagent kits (v2 Chemistry Dual index)	10x Genomics	PN-1000265; RRID: N/A

(*Continued on next page*)

Continued

REAGENT or RESOURCE	SOURCE	IDENTIFIER
CD8a (Ly-2) MicroBeads, mouse	Miltenyi Biotec	Cat#130-117-044; RRID: N/A
Deposited data		
ScRNA-seq	This paper	GEO: GSE217985
ATAC-seq	This paper	GEO: GSE217984
All experiments	This paper	GEO: GSE217986
Experimental models: Organisms/strains		
Wild-type C57Bl/6JOlaHsd	Envigo	RRID: IMSR_ENV:HSD-057
Pdcd1$^{-/-}$ *Pdcd1*$^{tm1.1Shr}$/J	Jackson Lab	Strain #:028276; RRID:IMSR_JAX:028276
CD45.1 mice B6.SJL-P*tprc*^{a} P*epc*^{b}/BoyJ	Jackson Lab	Strain #:002014; RRID:IMSR_JAX:002014
Eomesfl/fl B6129S1(Cg)-Eomes $^{tm1.1Bflu}$/J	Jackson Lab	Strain #:017293; RRID:IMSR_JAX:017293
CD4Cre+ (Tg(Cd4-cre)1Cwi/BfluJ)	Jackson Lab	Strain #:022071; RRID:IMSR_JAX:022071
OT1 ab$^{+/+}$C57BL/6-Tg(TcraTcrb)1100Mjb/J)	Jackson Lab	Strain #:003831; RRID:IMSR_JAX:003831
Rag2$^{-/-}$B6.Cg-Rag2 $^{tm1.1Cgn}$/J	Jackson Lab	Strain #:008449; RRID:IMSR_JAX:008449
C57BL/6_Eomes$^{tg/tg}$	Istaces et al.[70]	N/A
Software and algorithms		
FlowJo; v10.6.2	BD Biosciences	RRID: SCR_008520
FACS DIVA 9.0.1	BD Biosciences	RRID: N/A
MiXCR software v3.0.12	Bolotin et al.[71]	https://doi.org/10.1038/nmeth.3364 RRID: SCR_018725
VDJTools software v1.2.1	Shugay et al.[72]	https://doi.org/10.1371/journal.pcbi.1004503 RRID: N/A
Immunarch R package v0.7.0	ImmunoMind team[73]	https://github.com/immunomind/immunarch RRID: SCR_023089
Treemap R package v 2.4.3	N/A	https://cran.r-project.org/web/packages/treemap/index.html RRID: N/A
SeqMonk 1.43.0	Babraham Institute	https://www.bioinformatics.babraham.ac.uk/projects/seqmonk/RRID: SCR_001913
DeepTools 3.5.1 package	Ramírez et al.[74]	https://deeptools.readthedocs.io/en/develop/RRID: SCR_016366
Seurat 4.2.0 R package	Stuart et al.[75]	https://satijalab.org/seurat/;RRID: SCR_016341
Djvdj 0.0.0.9 R package	N/A	https://rnabioco.github.io/djvdj/index.html RRID: N/A
Slingshot (2.4.0)	Street et al.[53]	https://doi.org/10.1186/s12864-018-4772-0 RRID: SCR_017012
Monocle3 R package	Cao et al.[76]	https://doi.org/10.1038/s41586-019-0969-x RRID: SCR_018685
ScRepertoire(1.7.2) R package	Borcherding et al.[77]	https://f1000research.com/articles/9-47/v1 RRID: N/A
Circlize (0.4.15) R package	Gu et al.[78]	https://doi.org/10.1093/bioinformatics/btu393 RRID: SCR_002141
GraphPad Prism 8.0.2	GraphPad Software	RRID: SCR_002798
Cell Ranger v7.1	10x Genomics	https://www.10xgenomics.com/ RRID: SCR_017344

(*Continued on next page*)

Continued

REAGENT or RESOURCE	SOURCE	IDENTIFIER
Other		
Medium RPMI 1640 with L-Glutamine/ with 25mM HEPES	Lonza	Cat#BE12-115F; RRID: N/A
Fetal Bovine Serum; 5%	Sigma-Aldrich	Cat#F9665; Lot.BCBZ4242
L-Glutamine 200 mM in 0.85%NaCl solution; 1:100	Lonza	Cat#BE17-605^{E} RRID: N/A
NaPyruvate 100 mM solution; 1:100	Lonza	Cat#BE13-115^{E} RRID: N/A
NEAA Mixture (100x); 1:100	Lonza	Cat#13-114^{E} RRID: N/A
PEN-STREP 10.000 U Penicillin/mL; 1:100; 10.000 U Streptomycin/mL; 1:100	Lonza	Cat#DE-17-602^{E} RRID: N/A
2-Mercaptoethanol; 50μM	Sigmna-Aldrich	Cat#63689-100mL; CAS.n°: 60-24-2
Brefeldin A; 10μg/mL	Sigma	Cat#B6542; CAS.n°: 20350-15-6
Phosphate Buffered Saline	Lonza	Cat#BE17-516F; RRID: N/A
Ethylenediaminetetraacetic acid disodium salt solution	Sigma-Aldrich	Cat#03690; CAS n°:139-33-3
Novaseq 6000	Illumina	N/A
Bioanalyser High Sensitivity DNA Analysis Kit	Agilent	N/A
Chromium Controller	10xGenomics	N/A
DNase I, grade II	Roche	Cat#10104159001; RRID: N/A
Liberase Liberase^{TM} Research Grade	Roche	Cat#05401020001; RRID: N/A
Lymphoprep gradient	Stemcell Technologies	Cat# 07851; RRID: N/A
Percoll	Cytiva	Cat#VWR 17089101; RRID: N/A

RESOURCE AVAILABILITY

Lead contact

Further information and requests for resources and reagents should be directed to and will be fulfilled by the lead contact, Stanislas Goriely (stanislas.goriely@ulb.be).

Materials availability

This study did not generate new unique reagents.

Data and code availability

scRNA-Seq and ATAC-Seq data that support the findings reported in this study have been deposited in the GEO Repository. Accession numbers are listed in the key resources table. This paper does not report original code. Any additional information required to reanalyze the data reported in this paper is available from the lead contact upon request.

EXPERIMENTAL MODEL AND STUDY PARTICIPANT DETAILS

All experiments were performed on age- and sex-matched mice. Wild-type C57Bl/6 mice were purchased from Envigo (C57BL/6JOlaHsd). *Pdcd1*$^{-/-}$ mice were purchased from the Jackson Lab (*Pdcd1*$^{tm1.1Shr}$/J). CD45.1 mice under C57Bl/6 background were obtained from the Jackson Lab (B6.SJL-*Ptprc*^{a} *Pepc*^{b}/BoyJ). *Eomes*$^{fl/fl}$ mice under C57BL/6 background were purchased from the Jackson Lab (B6.129S1(Cg)-Eomes$^{tm1.1Bflu}$/J) and were crossed to CD4Cre^{+} mice obtained from the Jackson Lab

(Tg(Cd4-cre)1Cwi/BfluJ) to generate CD4Cre^{+}Eomes$^{fl/fl}$mice (i.e., the *de facto Eomes*$^{\Delta/\Delta}$mice). *Eomes* transgenic mice (*Eomes*$^{Tg/Tg}$) were generated as previously described.[70] *OT1*$\alpha\beta^{+/+}$*Rag2*$^{-/-}$*Eomes*$^{Tg/Tg}$ mice were generated by intercrossing OT1$\alpha\beta^{+/+}$ (C57BL/6-Tg(TcraTcrb)1100Mjb/J) and *Rag2*$^{-/-}$ (B6.Cg-*Rag2*$^{tm1.1Cgn}$/J), both purchased from the Jackson Lab, with *Eomes*$^{Tg/Tg}$ mice. Most experiments were performed on sex- and aged-matched mice between 6- and 12-weeks old. All animal work was carried out under SPF conditions and in compliance with and after approval by the institutional Animal Care and local committee for Animal Welfare from the Biopark ULB Charleroi (BUC).

METHOD DETAILS

Cell preparation

For all experiments, all organs were dissected and further processed under sterile conditions. Spleen were mashed and red blood cells were lysed using ACK (Ammonium-Chloride-Potassium, home-made) lysing buffer. Suspension were neutralized with RPMI 1640, 5% (v/v) FCS (Lonza) before further manipulation. Briefly, after perfusion and mechanical dissection, livers were cut and incubated for up to 30 min at 37 °C with Liberase (Liberase Research Grade (Roche, 05401020001) and DNase I, grade II (Roche, 10104159001), subsequently washed with RPMI1640, 5% (v/v) FCS (Lonza) and 2mM ethylenediaminetetraacetic acid (EDTA, Sigma), mashed and filtered through a 70 μm cell strainer. Next, samples underwent a Lymphoprep gradient (Stemcell Technologies, Catalog # 07851) (6 mL lymphoprep/4 mL cell suspension in HBSS (Lonza)) and centrifugation for 20 min at 2000 rpm at 20°C without break. Lymphocytes were then collected at the interface, washed, and counted if necessary. T cells from lungs were obtained by first flushing the lungs, after dissection, the lungs are digested enzymatically (same procedure as the livers), mashed and filtered through a 70 μm cell strainer. Lymphocytes were recovered at the interface after a (40%/70%) Percoll gradient (Cytiva, VWR 17089101). Thymuses and lymph nodes were dissected, mashed, and filtered. Thymocytes and lymphocytes from lymph nodes were harvested without further processing. Bone marrow cells were harvested by dissecting the two inferior limbs of the mice (femur and tibia), harvesting bone marrow and cell suspension were recovered after red blood lysis with ACK.

Flow cytometry staining

Single-cell suspensions were stained to exclude dead cells (ViaKrome 808 Fixable Viability Dye from Beckman Coulter C36628 or LIVE/DEAD Fixable Aqua Dead Cell Stain Kit, for 405 nm excitation, Life Technologies) and incubated with rat anti-mouse CD16/CD32 (BD, clone 2.4G2, dilution 1:100, catalog 553141) and a surface antibody mix prepared in brilliant stain buffer (BD) for 20 min at 4 °C in the dark. For intracytoplasmic or intranuclear staining, cells were fixed and permeabilized for 30 min at 4 °C in the dark (eBioscience Foxp3/Transcription Factor Staining Buffer Set, Life Technologies, 00-5523-00) before staining (30 min at 4 °C in the dark). Cells were stained with the fluorochrome conjugated monoclonal antibodies indicated in the STAR Methods. Flow cytometry data were acquired on a Cytoflex LX or Cytoflex S and data were analyzed using FlowJo (v10.6.2).

To evaluate the clonality of the T cells we used the Anti-Mouse TCR Vβ Screening Panel (557004) from BD. The H-2Kb/SIINFEKL tetramer conjugated to phycoerythrin (PE) was purchased from ProImmune (F093).

Cell cultures and *ex vivo* stimulations

All cell cultures were performed in complete medium (RPMI 1640 with 5% (v/v) FCS, 2 mM L-glutamine, 1 mM sodium pyruvate, 0.1 mM non-essential amino acids, 40 mM β-mercaptoethanol, 100 U ml^{-1} of penicillin, and 100 U ml^{-1} of streptomycin (all reagents from Lonza) at 37 °C and 5% CO2. Lymphocytes were cultured for 4 h in the presence or absence of phorbol-myristate-acetate (50 ng mL−1, Sigma, 79346) and ionomycin calcium salt (1 μg mL^{-1}, Sigma, I3909), brefeldin A (10 μg mL−1, Sigma, B6542) being added for the last 3 h before staining.

Adoptive transfer experiment

Splenic CD8^{+} T cells were purified by negative selection (Dynabeads Untouched Mouse CD8 Cells Kit, Life Technologies). Purified CD8^{+} splenocytes were stimulated for 48h in presence of anti-CD28 (1μg/mL) and IL-2 (10 ng/mL) in anti-CD3 (1μg/mL) coated 24-well plates. After stimulation, cells were harvested, counted and intravenously injected in congenic mice.

Anti-PD-1 treatment

The different mice strains were treated intraperitoneally with anti-PD-1 anti-mouse antibody (clone RPM1-14 from BioXcell (BE 0146), 200μg/mice) for 2 weeks every 2–3 days (for a total of 6 injections).

Gini TCR skewing index

The Gini Index is used in economic statistics and can also be applied in TCR repertoire analysis by flow cytometry. The Gini TCR skewing Index allows to calculate the TCR-Vβ distribution among T cells. Proportions of all 15 TCR-Vβ families within each T cell subset were calculated and arranged from small to large.

L. monocytogenes infection

C57BL/6 or *Eomes*$^{Tg/Tg}$ mice were challenged intravenously with 5.10^5 (500.000 CFU/mice) attenuated *Listeria Monocytogenes* strain expressing OVA (*Lm-OVA*$^{\Delta Acta}$) kindly provided by Dr Hao Shen, Department of Microbiology, University of Pennsylvania School of Medicine, Philadelphia.[69] Mice were sacrificed and cells harvested 40 days after challenge.

Cell sorting

Hepatic T cells were enriched as previously described (cell preparation section). Splenic CD8$^+$ T cells were purified by negative selection (Dynabeads Untouched Mouse CD8 Cells Kit, Life Technologies) resuspended in phosphate buffered saline (PBS, Lonza) with 5% (v/v) FCS and 2 mM EDTA. Thymocytes were prepared as previously described (flow cytometry section). Enriched cells were stained to exclude dead cells and incubated with Fc receptor-blocking antibodies and a surface staining antibody mix (BDBiosciences): CD8α-BV510 (563068), TCRβ PerCP-Cy5.5 (560657), CD4-PE (553049). TCRβ$^+$ CD8α $^+$ CD4$^-$ cells were sorted on a BD FACSAria III.

Bulk TCR-sequencing

CD8SP thymocytes and Spenic or hepatic CD8$^+$ T cells were sorted before performing bulk TCR-sequencing from 5 WT mice and 5 mice treated with anti PD-1 treatment. Remaining CD8$^+$ T cells from the liver of 4 treated animals were further subsorted into two groups, PD-1 ^{lo} CD8$^+$ and PD-1^{hi} CD8$^+$ T cells. RNA extraction was carried out using the RNeasy Micro Kit (Qiagen, 217084) according to the manufacturer's instructions from samples ranging from 17.000 to 25.000 sorted cells. Furthermore, blood before and after treatment was collected in PAXgene Blood RNA tubes and RNA was extracted with PAXgene Blood RNA Kit (Qiagen, 762164). Template-switch-anchored RT-PCR and high-throughput sequencing was performed as previously described.[79] Raw sequencing fastq files were successfully obtained (except for 1 PD-1^{lo} sample) and aligned with the GenBank reference V, D, and J genes to extract TRA and TRB CDR3 sequences using MiXCR software (version 3.0.12).[71] The CDR3 sequences were analyzed using VDJtools software (version 1.2.1)[72] and Immunarch R package (version 0.7.0).[80] Out-of-frame sequences were excluded from the analysis, as well as nonfunctional TRA and TRB segments using IMGT (the international ImMunoGeneTics information system) annotation. Tree maps were generated using the Treemap R package (version 2.4.3) and diversity was calculated with the D75 metric index by measuring the percentage of clonotypes required to occupy 75% of the total TCR repertoire. Other diversity read-outs were obtained from the resampled file generated using CalcDiversityStats function from VDJtools. Finally, the sharing of repertoire was assessed using the output of CalcPairwiseDistances from VDJTools. This last analysis performs an all-versus-all pairwise overlap and to illustrate the repertoire sharing between PD-1^{hi} samples we used the sum of relative abundances of shared sequences between the two pairs of each comparison.

ATAC-sequencing

For library preparation, nuclei from 20,000 cells (liver WT CD8$^+$ T cells/PD-1^{hi} or PD-1^{lo} from *Eomes*$^{Tg/Tg}$) were subject to transposition reaction in 1x TD buffer containing 2.5 μL transposase Nextera enzyme (Nextera DNA sample prep kit, Illumina) and DNA was purified using MinElute PCR Purification Kit (Qiagen). Purified DNA was amplified by PCR using NEBNext High-Fidelity 2 × PCR Master Mix (New England Biolabs) with 10–12 cycles. Amplified libraries were purified using MinElute PCR Purification Kit (Qiagen) and quality controlled using a Bioanalyzer High-Sensitivity DNA Analysis kit (Agilent). Paired-end sequencing was performed on NovaSeq 6000 (Illumina). Paired-end reads were mapped to mouse genome mm10 with Bowtie2 using default parameters for paired-end reads. Reads that mapped several regions, or with insufficient mapping quality, were removed with samtools view. We also removed reads located within the blacklist of the ENCODE project48. Duplicate reads were removed with MarkDuplicates tools (Picard suite). Peaks were called with MACS2 using the following parameters: -f BAMPE -g mm -q 0.05 –nomodel –call-summits -B –SPMR. Regions obtained from the three populations were subjected to differential analysis using SeqMonk 1.43.0 (Mapped Sequence Analysis Tool, Babraham Bioinformatics, http://www.bioinformatics.babraham.ac.uk/projects/seqmonk/). First, we created an atlas containing all obtained peaks for all the populations with a minimum overlap of 1 bp. Regions with differential accessibility were obtained using DESeq2 with a significance below 0.05 after Benjamimi and Hochberg correction with the application of independent intensity filtering. Fordownstream visualization, a scaling factor was calculated using deepTools 3.5.1 package to normalize peak intensity to FRiP (fraction of reads in peaks) and generate bigwig files. For Gene ontology analysis, we introduced BED files resulting from the overlap between differentially accessible regions in CD8$^+$ T cells/PD-1^{hi} from *Eomes*$^{Tg/Tg}$ and EOMES ChIP-seq (GEO: GSE126770) to the GREAT tool[81] using Basal plus extension mode option modified to 300kb. Ciiider algorithm[82] (http://ciiider.com/) was used to perform motif enrichment in the differentially accessible regions of *Eomes*$^{Tg/Tg}$ PD-1^{hi} vs. PD-1^{lo}.

scRNA-sequencing and scTCR-sequencing

Single-cell suspension from splenocytes and liver T cells from six C57BL/6 mice and three *Eomes*$^{Tg/Tg}$ and *Pdcd1*$^{-/-}$ mice were obtained as described. For *Eomes*$^{Tg/Tg}$ mice, cells were pooled and CD8$^+$ T cells from spleens and livers were sorted. For *Pdcd1*$^{-/-}$, cells from 3 mice were labeled using TotalSeq-C barcoded anti-mouse hashtag antibodies (Biolegend) and CD8$^+$ T cells from individual spleens and livers were sorted. Microscope assessment after Trypan blue staining allowed to count viable cells following FACS sorting. Cell preparations were centrifuged at 500 RCF for 7 min and pellets were resuspended in 10%FCS/RPMI medium. Cells were loaded on the Chromium Controller (10x Genomics) and Single-cell RNA-seq libraries were prepared using the Chromium Single Cell

5′ v1.1 (*Eomes*$^{Tg/Tg}$) and v2 (*Pdcd1*$^{-/-}$) reagent kits (10x Genomics) according to manufacturer's protocol. Libraries were loaded to an Illumina Novaseq (Brightcore platform, http://www.brightcore.be/), and Cell Ranger (10x Genomics) functions mkfastq and multi were used to align to the mm10 genome and demultiplex the sequencing data and generate gene-barcode matrices. Resulted matrices were used to generate a single seurat object using Seurat 4.2.0 R package. To integrate TCR information generated by Cell Ranger we used djvdj 0.0.0.9 R package. Cells with >12% of mitochondrial read and <300 and >4000 detected genes were filtered out. To analyze the resulted seurat object we followed the integration workflow as described by Stuart et al.[75] Briefly, anchors between different conditions were identified by calling *FindIntegrationAnchors ()* function and creation of integrated assay using *IntegrateData ()* function. Then, features were scaled, and centered and top 30 principal component (PCs) were used in UMAP analysis to identify clusters using the original Louvain algorithm with a resolution of 0.5. We applied *FindAllMarkers ()* function to identify differentially expressed genes in each cluster as compared to all other clusters (Wilcoxon Rank-Sum test). The differentially expressed genes were used to annotate cells populations. *AddModuleScore ()* function was used with default parameters to calculate Tex, Trm and TEM signatures scores coming from public scRNAseq dataset.[51,52] Slingshot (2.4.0) and monocle3 R packages were used to perform trajectory analysis on the integrated seurat object or separated two seurat objects (WT and *Eomes*$^{Tg/Tg}$).

To analyze TRC repertoire, we used scRepertoire (1.7.2) R package. Briefly, we introduced the ''filtered_contig_annotations.csv'' output from the 10x Genomics Cell Ranger and analyzed the clonotype dynamics and diversity in each mouse strain. In addition, we combined TCR repertoire data with the integrated seurat object and analyzed the distribution of clonotypes. Interconnection between the annotated populations was evaluated and showed by chord diagrams using circlize (0.4.15) R package.

QUANTIFICATION AND STATISTICAL ANALYSIS

Prism 8.0.2 was used for statistical analysis. Mann–Whitney test was used to compare two datasets. Kruskal-Wallis test was used to compare three or more datasets. Statistical details can be found in the figure legends.